p53 translational-isoform Δ40p53 regulates cell cycle by modulating the miR-4671-5p/SGSH axis

Apala Pal[1], Pritam Kumar Ghosh[1], Sahana Ghosh[2], Sachin Kumar Tripathi[1], Sohini Guha[3], Pragnya Coca[4], Subrata Patra[2], K.M. Prathima[5], Debjit Khan[1,6], Manjula Das[3,7], Arindam Maitra[2] and Saumitra Das[1,] *

[1]Department of Microbiology and Cell Biology, Indian Institute of Science, Bangalore-560012, India.

[2]National Institute of Biomedical Genomics, Kalyani-741251, India.

[3]Molecular Immunology, Mazumdar Shaw Medical Foundation, Narayana Health City, Bommasandra, Bangalore-560099, India.

[4]Mazumdar Shaw Medical Center, Narayana Health City, Bommasandra, Bangalore-560099, India.

[5]Manipal Hospital, Miller's Road, Bangalore-560052, India.

[6]Department of Life Sciences, GITAM School of Science, GITAM (Deemed to be University), Bangalore-562163, India.

[7]Center for Precision Diagnostic and Therapeutic Research, India (CPDTRI), Electronic city, Bangalore-560100, India

*Address for correspondence:

Dr. Saumitra Das, Professor,

Department of Microbiology and Cell Biology,

Indian Institute of Science, Bangalore-560012, India

Email: sdas@iisc.ac.in

Phone: 91 80 2293 2886

Fax: 91 80 2360 2697

ABSTRACT

Parsing functions of tumour suppressor gene *TP53* is inherently complicated owing to multiple p53 isoforms it encodes. Δ40p53, the only translational isoform, alters p53 target gene expression both positively and negatively, thereby modulating p53 functional activity. Independent of p53, Δ40p53 regulates miR-186-5p–YY1 axis to decrease cell proliferation. To uncover miRNAs that are differentially regulated by Δ40p53 and p53, in this study, we performed small RNA sequencing. Overexpression of Δ40p53, but not full-length (FL) p53, substantially downregulated expression of miR-4671-5p. However, upon overexpression of different ratios of Δ40p53 and FLp53, changes in miR-4671-5p levels implied that it is a FLp53 modifiable target. In an *in-silico* approach, we identified N-sulfoglucosamine sulfohydrolase (*SGSH*) as a candidate miR-4671-5p target. We provide evidence that miR-4671-5p directly binds to *SGSH* 3'UTR, degrading its RNA and consequently decreasing protein levels. Further, our findings indicate that Δ40p53 expression level in a cohort of colorectal cancer patient samples can stratify miR-4671-5p and *SGSH* mRNA expression, with inverse correlation of miR-4671-5p and *SGSH*. Importantly, overexpression of miR-4671-5p triggered intra-S-phase cell cycle arrest. Thus, Δ40p53-miR-4671-5p-SGSH axis emerges as a novel axis capable of regulating cell cycle progression. SGSH gene expression levels depict potential prognostic relevance on survival that trends oppositely to miR-4671-5p levels associated with the same cancer types, supporting a direct physiological relevance of the interaction. Collectively, these findings significantly broaden understanding of functions of Δ40p53 that are mediated by miRNAs to help maintain metabolic and cellular homeostasis independently of FLp53.

Keywords: p53 isoform, Δ40p53 role, miR-4671-5p expression, SGSH role in cell cycle regulation

INTRODUCTION

Cellular stress responses are multifaceted and involve damage recognition and repair, including that of DNA, to minimize the risk of genetic instability [1]. p53 binds DNA and plays a central role in protecting genomic integrity. Under genomic stress, p53 causes cell cycle arrest and hinders the proliferation of cells with damaged DNA [2]. The functional activities of p53 are lost in multiple human cancers due to protein inactivation or gene mutations [3]. The p53 pathway is regulated by several factors, among which the role of p53 isoforms is crucial because these can alter transcriptional activation of p53 targets and thus affect its functions [4]. Twelve p53 isoforms are produced via various mechanisms to bear N-terminal (FL/Δ40/Δ133/Δ160) and C-terminal (α/β/γ) diversity [5], and each is differentially expressed in normal and tumor tissues in various types of cancer [6, 7]. Among these, the only translational isoform of p53 is Δ40p53, and it critically sculpts p53 functions [8]. We previously identified two internal ribosome entry sites (IRESs) within p53 mRNA, where one IRES generates the full-length p53 (FLp53) protein, whereas initiation at the other generates Δ40p53 [9]. We have also shown that several translation initiation factors are critical for the differential regulation of IRES activity under various types of stress [10, 11].

FLp53 has a strong affinity for, and can form homo-tetramers and hetero-tetramers with Δ40p53, because they share oligomerization domains [12]. Furthermore, Δ40p53 can regulate the functional activity of p53, which directly affects cellular processes [13], as well as critical cellular processes, such as the cell cycle, proliferation, and senescence. The IRESs driving p53 isoforms have different cell cycle phase-dependent activities, with IRES for FLp53 being active at the G2–M transition and IRES for Δ40p53 being the most active at the G1–S transition [9]. In addition to regulating p53 activity, Δ40p53 retains the second transcriptional activation domain in FLp53 and induces the expression of various genes independently of FLp53,— [14, 15, 16]. Δ40p53 also induces 14-3-3σ and G2 arrest but does not affect G1 progression [17, 18]. It transactivates Bcl-2 Associated X-protein and Growth Arrest and DNA Damage-inducible 45 in p53-null cells [8]. The Nanog-IGF1 axis is also modulated by Δ40p53/FLp53 hetero-oligomers, thus controlling the switch from pluripotency to differentiation [19]. The proliferation of pancreatic β cells and glucose homeostasis is controlled by Δ40p53 in mice [20]. At basal levels, Δ40p53 and p53 similarly suppress cellular mobility and proliferation in breast cancer [21]. We found that Δ40p53 (and not FLp53) uniquely regulates miR-186-5p, which can downregulate expression of the known oncogene Ying

Yang 1 (YY1) protein, thereby decreasing cell proliferation [22]. In another study we have also found that Δ40p53 regulates lncRNA (LINC00176) which can control cell fate mediated through multiple miRNA and mRNAs [23]. Contrary to its tumor suppressive role Δ40p53 independently activates the netrin-1 promoter and promotes cell survival [24].

This study aimed to globally identify those miRNAs that are differentially regulated by Δ40p53(α) and p53(α). We assessed changes in miRNA expression in lung and colon cancer cell lines cells expressing either or both FLp53(α) and Δ40p53(α) to identify such differential miRNA regulation.

MATERIALS AND METHODS

Cell lines and transfections

We have used three cell lines in the current study: H1299 (lung adenocarcinoma cell line lacking p53 or Δ40p53), HCT116 p53+/+ cells (colon carcinoma cell line harboring wild-type p53; hereafter called HCT116+/+); and HCT116 p53-/- cells (colon carcinoma cell line harboring only Δ40p53; hereafter called HCT116-/-). These cells were maintained in DMEM (Sigma) with 10% Foetal Bovine Serum (GIBCO, Invitrogen). 70%-80% confluent monolayer of cells was transfected with various plasmid constructs using Lipofectamine 2000 (Invitrogen) and Turbofectamine in Opti-MEM (Invitrogen). The medium was replaced with DMEM (with antibiotic) and 10% FBS four hours later. The cells were harvested and processed as required at the desired time point.

Small RNA Sequencing

RNA Extraction: Total RNA was isolated from control (only vector), p53, Δ40p53, 14A (p53 and Δ40p53) transfected H1299 cells using TRIzol and PureLink RNA mini kit (Ambion) according to the manufacturer's instructions. Quality of isolated total RNA was checked using Agilent RNA 6000 Nano chips in 2100 Bioanalyzer (Agilent) and NanoDrop spectrophotometer (Thermo Scientific) and quantitation was performed in Qubit using Quant-iT RNA assay kit broad range (Thermo Scientific). Total RNA samples with RNA integrity number (RIN) >7 was selected for Illumina small RNA sequencing library preparation.

Library Preparation: Small RNA sequencing library preparation was performed using Illumina® TruSeq® Small RNA Library Prep Kit according to the manufacturer's protocol.

One microgram of the total RNA sample was used for library preparation, and adapters were ligated to 3' and 5'ends of each RNA molecule. Subsequent reverse transcription and amplification were performed to generate a cDNA library, which was further gel purified to select bands between 145-160 bp to prepare a final small RNA sequencing library for clustering and sequencing. Single read 1 x 50 bp sequencing of these libraries was performed in HiSeq-2500 (Illumina).

RNA-seq data analysis: FASTQ files generated for each sample were checked for quality, and then adapter trimming was performed using the cutadapt2 tool (v1.8.1). Adapter trimmed FASTQ files were aligned to the hg19 reference sequence using the mapper module of the miRDeep2 software package. The accepted aligned FASTA files were processed using miRDeep2 module where known mature, precursor miRNAs from humans and mature miRNAs from other species were provided (downloaded from miRBase database) as input. It identified known and novel miRNAs expressed. miRDeep2 module quantifies the expression of the known miRNAs and gives normalized read counts (reads per million: RPM) for each known precursor miRNA. Average RPM values were calculated where a single mature miRNA had multiple precursor miRNAs. DESeq2 was used to identify differentially expressed miRNAs.

Plasmids and constructs

pGFP-hp-p53- 5'UTR-cDNA (14A): It expresses both FLp53 and Δ40p53 (a generous gift from Dr. Robin Fahraeus, INSERM, France). pGFP-hp-p53-5'UTR (A135T)-cDNA which expresses only Δ40p53 and pGFP-hp-p53- 5'UTR (A251G/T252 C/G253T)-cDNA which expresses only full-length p53 (p53FL) [22]. miR 4671-5p and miR-34a-5p overexpression construct cloning were done by annealing double-stranded oligos of a mature miR-4671-5p and miR-34a-5p respectively, along with the hairpin sequence in the middle between BglII and XhoI in pSuper vector. pCD-Luc-SGSH-3'UTR and pCD-Luc-CDK5R1-3'UTR containing SGSH and CDK5R1 3'UTRs (respectively) were used in the study. They were cloned between XhoI and XbaI downstream of the luciferase gene in the pCD-Luc vector. pCD-Luc-SGSH-3'UTR mutant and pCD-Luc-CDK5R1 mutant have been used. Both the mutants containing 3'UTRs with a mutation in the miR-4671-5p binding site were used in the luciferase experiments.

siRNA transfections

HCT116+/+ and HCT116-/- cells were transfected with 30 nM si p53 RNA (IDT). 5'-AACCUCUUGGUGAACCUUAGUACCU-3' is the sequence for p53 siRNA, directed against the 3'UTR of p53; therefore, it targets both p53 as well as Δ40p53. In the experiments, a non-specific siRNA (Dharmacon) was used as a control.

Western Blot analysis

Protein concentrations of the extracts were assayed by Bradford (Bio-Rad), and equal amounts of cell extracts were separated by SDS 12% PAGE and transferred to nitrocellulose membrane (Bio-Rad). Samples were then analyzed by Western blotting using a rabbit-raised anti-p53 polyclonal antibody (CM1, a kind gift from Dr. Robin Fahraeus, INSERM, France and Prof. J.C. Bourdon, of University of Dundee, UK), followed by secondary antibody (horseradish peroxidase-conjugated anti-mouse or anti-rabbit IgG; Sigma). SGSH protein has been detected using anti-SGSH Antibody (Abclonal, Cat. No. A8148). CDK11B protein has been detected using anti-CDK11B Antibody (Abclonal Cat. No. A12830). CDK5R1 protein has been detected using anti-CDK5R1 Antibody (Abclonal Cat. No. A14497). Densitometric analysis was done on Fiji (https://fiji.sc/) by calculating band intensity and deducting the averaged background value from equal areas at the top and bottom of the band.

RNA isolation and Real-time PCR

According to the manufacturer's protocol, total RNA was isolated from cells with TRI Reagent TM (Sigma). The isolated RNA was treated with 10 units of DNase I (Promega), extracted with acidic phenol-chloroform, and precipitated with 3 M sodium acetate (pH 5.2) and 2.5 volumes of absolute alcohol. RNA amount was quantified with Nano-spectrophotometer, and cDNAs were synthesized using specific reverse primers and MMLV RT (Revertaid ™ Thermo Scientific) at 42°C for 1 h, according to standard protocol. At the same time, 2-5μg of total RNA has been used to check mRNAs' expression. 50ng of total RNA has been used to check the expression of miRNAs.

SYBR green Assay System was used for mRNA, lncRNA and miRNA detection and quantification. We have used actin as an endogenous control for mRNA and 5SrRNA as an endogenous control for miRNAs. The thermocycling conditions for SYBR green Assay system include 1 cycle of 95°C for 10 min, 40 cycles of 95°C for 15 s, 60°C for 30 s and 72°C for 30 s (Applied Biosystems). $2^{-\Delta\Delta Ct}$ method algorithm was used to analyze the relative

changes in expressions, where actin/5S served as an endogenous control. The fold change was calculated using $2^{-\Delta\Delta Ct}$. ΔCt = Ct (target gene) −Ct (endogenous control) and ΔΔCt = ΔCt target sample) −ΔCt (control sample). For patient samples, normalized m gciR-4671 (ΔCt) = Ct (miR-4671) −Ct (U6 snRNA) and normalized mRNA of (ΔCt) = Ct (mRNA) −Ct (actin). Melting curve analysis of every (q)PCR was conducted after each cycle.

Luciferase Assay

According to the manufacturer's protocol, Firefly luciferase activity was measured using Dual-Luciferase Reporter Assay System (Promega, USA Cat#1910). The transfected cells were harvested in Passive lysis buffer (PLB) after 48 hours of transfection, and luciferase activity was measured.

Cell cycle Analysis

HCT116-/- cells were transfected with miR-4671-5p or miR-34a-5p overexpression construct 48 h post-transfection; the cells were harvested and fixed with methanol. The fixed cells were treated with RNase A (10 mg/ml) for 1 h at 37°C, following which PI (Propidium iodide-1mg/ml) was added to the cells and taken for Flow cytometric analysis.

Bioinformatic Analysis

dbDEMC2.0 (https://www.biosino.org/dbDEMC/index) has been used to perform a meta-profiling of selected miRNAs [25]. TargetScan 7.2 (https://www.targetscan.org/vert_72/) has been used to predict target mRNAs of miRNAs [26]. miRDB has been used to predict target miRNAs (https://mirdb.org/cgi-bin/search.cgi) [27, 28]. GO-term analysis was done on PANTHER release 17.0 (http://www.pantherdb.org/). Kaplan-Meier survival analysis was done on R2: Genomics Analysis and Visualization Platform (http://r2.amc.nl). Heat map for Figure 1E has been generated using Heatmapper (http://heatmapper.ca/).

Collection, processing, and analysis of colorectal carcinoma samples

Sample collection: Tumor samples, with informed consent [approval no. NHH/AEC-CL-2020-458 of ethics committee of Narayana HealthBangalore, India] from patients were cut into 3-5 small sections weighing ~30 mg and snap frozen in liquid nitrogen for storage The clinical and pathological details of the patients are mentioned in **Figure S1, Table 1**.

RNA isolation: RNA was isolated from fresh frozen tissue samples using TRIzol (Ambion, #15596018) as per manufacturer's instructions. Briefly, ~30 mg of the fresh frozen tissue

samples were minced and dissolved in 1 ml TRIzol followed by addition of 200 µl of chloroform (Sigma, #496189) and centrifugation at 13,000 g for 15 minutes at 4°C. The aqueous layer was transferred to a fresh tube containing an equal volume of 100% isopropanol (Qualigen, #Q26897) without disturbing either the middle interface or the lower organic phase. The tube was gently invert-mixed and incubated at room temperature for 10 minutes followed by centrifugation at 13,000 g for 10 minutes at 4°C. The supernatant was discarded, and the pellet was washed with 75% ethanol (HiMedia, #MB228) followed by centrifugation at 7500 g for 5 minutes at 4°C. The pellet was air dried and resuspended in nuclease free water (Ambion, AM9937) for further processing.

Protein isolation and Quantification: Protein was isolated from a fresh frozen tissue piece of ~30 mg using NucleoSpin RNA/Protein purification kit (Macharey-Nagel, #740933.5), as per manufacturer's instructions. Quantification was done using the Pierce BCA protein assay kit (ThermoScientific #23227) as per manufacturer's instructions. Absorbance was measured at 562 nm.

Histopathology analysis: Tumor tissues fixed in 10% (v/v) formalin (Sigma, #HT501128) and embedded in paraffin (Qualigen, #Q19215) were used in the study. Sections of 5 µm thickness were stained with hematoxylin and eosin. Slides were analysed for the extent of tumor boundary and regions of necrosis.

Statistical analysis

The data for the experimental section are expressed as mean ± SD. Statistical significance for the experiments was determined using two-tailed Student's t-test. The criterion for statistical significance was $p \leq 0.05$ (*) or $p \leq 0.01$ (**) or $p \leq 0.001$(***)

RESULTS

Small RNA sequencing reveals miRNA targets of p53 and Δ40p53

H1299 cells (that do not endogenously express any p53 isoforms), were transfected with vectors (in triplicate) to ensure that they expressed only FLp53, only Δ40p53, both p53 and Δ40p53 (vector 14A), or GFP (Control, C) **(Figure 1A-C)**. We then investigated the effect of differential expression of p53 isoforms on miRNA gene expression using RNA isolated from these cells and processed for quality control and sequencing of small RNAs. A heatmap was

generated for those miRNAs with unidirectional fold changes for at least one condition of p53 isoform overexpression, in all triplicates, compared to control **(Figure 1D)**. Among 135 miRNAs, we selected a significantly expressed cluster which is differentially regulated under at least one condition. ($p \leq 0.05$; **Figure 1E**).

We primarily aimed to identify miRNAs with an expression that was differentially regulated by p53 and Δ40p53 and thus selected miR-4671-5p, miR-301b-5p, miR-34a-5p, and miR-548ae-5p, with fold changes ranging between ≥ 0.58 and < -1.0 ($p \leq 0.05$). The expression of miR-4671-5p was significantly downregulated and was unchanged on the Δ40p53 and p53 backgrounds, respectively. The expression miR-301b-5p was significantly downregulated and unchanged on the p53 and Δ40p53 backgrounds, respectively. We also analysed the novel miR-548-ae-5p, the expression of which was significantly upregulated by p53 and the other two conditions. We then investigated the mechanism of co-regulation by the isoforms (if any) on miR-548ae-5p, and the positive control was miR-34a-5p that is regulated by p53 [29].

Selection and validation of miRNAs for further studies

Control (vector only), p53, Δ40p53, and 14A (a combination of both isoforms) were transfected in H1299 cells **(Figure 2A)** and the miRNA levels were examined using qRT-PCR. The expression of miR-4671-5p decreased when Δ40p53 and 14A were overexpressed and remained unchanged upon p53 overexpression compared with controls **(Figure 2B)**. The expression of miR-34a-5p and miR-548ae-5p increased when p53, Δ40p53, and 14A were overexpressed **(Figure 2C and D)**. The expression of miR-301b-5p was not altered by overexpressed p53, whereas overexpressed Δ40p53 and 14A increased it **(Figure 2E)**. Except for miR-301b-5p, the expression of miR-4671-5p, miR-548ae-5p, and miR-34a-5p was similar to that obtained using the sequencing platform **(Figure 2F)**. Therefore, we continued our investigation with these three miRNAs.

Regulation of miRNAs by Δ40p53 and p53

Colon cancer cell lines HCT116+/+ (predominantly expressing p53 and some Δ40p53) and HCT116-/- (expressing only 40p53) were used to determine how p53 isoforms regulate the expression of these miRNAs and to render our study more physiologically relevant **(Figure 3A)**. We initially found less endogenous expression of miR-4671-5p and more miR-548ae-5p and miR-34a-5p in HCT116-/-, than HCT116+/+ cells **(Figure 3B)**. Furthermore, p53 or Δ40p53 was partially silenced by siRNA-mediated knockdown in HCT116+/+ **(Figure 3D)**

and HCT116-/- **(Figure 3F)** cells and miRNA levels were detected using qRT-PCR. The expression of miR-548ae-5p and miR-34a-5p significantly decreased upon silencing p53 or Δ40p53 in HCT116+/+ cells, whereas that of miR-4671-5p did not significantly change **(Figure 3 C)**. Silencing Δ40p53 increased miR-4671-5p and decreased miR-548ae-5p and miR-34a-5p expression in HCT116-/-cells. These data suggested that Δ40p53 regulates miR-4671-5p negatively and miR-548ae-5p and miR-34a-5p positively **(Figure 3E)**. Importantly, Δ40p53 exclusively altered miR-4671-5p expression, with no effect by FLp53. These results also indicated that changing relative p53 and Δ40p53 levels differentially affects miRNA expression. The abundance of p53 isoforms notably differs among various types of cancer [6]. Therefore, target miRNAs should vary accordingly.

Bioinformatic analysis of miR-4671-5p, miR-548ae-5p, and miR-34a-5p expression in various types of cancer using the database of differentially expressed miRNAs (dbDEMC) 2.0 revealed that miR-34a-5p is expressed in many types of cancer, whereas miR-4671-5p is expressed only in colon, lung, and pancreatic cancers. In contrast, miR-548ae-5p was not detected in any cancer databases **(Figure 4A)**. The results indicated that the varying levels of miRNAs among types of cancer could be attributed to the varying abundance of p53 and Δ40p53. To confirm this, we overexpressed p53 or Δ40p53 at different ratios in H1299 cells and measured the expression of these miRNAs **(Figure 4B)**. We found that miRNA expression significantly changed according to the abundance of p53 or Δ40p53. The expression of miR-34a-5p was upregulated by either overexpressed p53 or Δ40p53. However, different ratios of both p53 and Δ40p53 isoforms decreased miR-34a-5p expression, whereas equal amounts did not cause any changes **(Figure 4C)**. These results agree with previous findings suggesting that p53 and Δ40p53 co-regulate their activities, thus leading to the modulation of target gene expression [12].

Furthermore, overexpressed FLp53 did not significantly change miR-4671-5p expression, which was (similar to our findings in **Figure 2A**). However, increasing Δ40p53 levels in the absence or presence of FLp53 consistently decreased miRNA expression **(Figure 4D)**. The combined effects of these isoforms on the expression miR-4671-5p and 14A were similar. Thus, in the context of miR-4671-5p, p53 might act as a regulator of the Δ40p53-mediated gene expression. However, p53 alone did not affect miR-4671-5p.

Effect of miR-4671-5p on its target mRNAs

Micro RNAs function by base pairing with their target mRNAs and negatively regulating their expression. The miR-34a family is regulated by p53 and miR-34a-5p is involved in multiple cellular processes[29]. However, miR-4671-5p is novel, and its regulation has remained unknown. Therefore, we investigated miR-4671-5p and elucidated its downstream functions using the online databases Human TargetScan 7.2 and miRDB to identify potential mRNA targets of miR-4671-5p. These two databases respectively provided 780 and 46 targets **(Figure S1, Table 2)**. 40/46 targets from miRDB targets were found in the TargetScan database and 6/46 were absent. Next, we performed GO term analysis by PANTHER statistical overrepresentation test using the curated 786 unique-target gene. GO molecular function "protein serine kinase activity" was significantly enriched in the predicted target list of miR-4671-5p that includes multiple kinases **(Figure S1, Table 3)**.

CDK11B (Cyclin Dependent Kinase 11B) and CDK5R1 (Cyclin Dependent Kinase 5 Regulatory Subunit 1) were selected as potential miR-4671-5p targets **(Figure 5A)**. Importantly, PANTHER analysis showed an overrepresentation of serine kinases as predicted targets of miR-4671-5p, highlighting the relevance of selecting these candidates **(Figure S1, Table 3)**. Further, we also shortlisted SGSH (N-Sulfoglucosamine Sulfohydrolase) as it is the topmost target for miR-4671-5p in Targetscan. Mutations in SGSH cause a lysosomal sulfite enzyme deficiency that leads to glycosaminoglycan (GAG) and heparan sulfate accumulation in various organs of the body, ultimately causing mucopolysaccharidosis III A (MPS) syndrome that is characterized by sever neurological symptoms and skeletal deformities [30]. While an association of SGSH to monkeypox and interstitial lung disease has been predicted [31, 32] a role for SGSH in cancer is yet unknown. An analysis of existing primary tumor datasets for SGSH gene expression revealed that low *SGSH* is significantly correlated with poor survival in pancreatic adenocarcinoma **(Figure 5B and Figure S1-Table 4)** in 3/4 datasets, while high *SGSH* is significantly correlated with poor survival in multiple colon tumor datasets **(Figure 5C)**. Importantly, in these tumor types, prognostic *SGSH* levels trend opposite to miR-4671-5p as revealed in dbDEMC2.0 analysis **(Figure 4A)** suggestive of a link between the miRNA and mRNA. Thus, SGSH, CDK11B and CDK5R1 were selected for further studies.

We validated miR-4671-5p target levels under the same experimental conditions as in Figure 4B, with different ratios of overexpressed p53/Δ40p53 in H1299 cells. The results showed

increased SGSH, CDK11B, and CDK5R1 levels only under Δ40p53 overexpression **(Figure 5D-F)**. Moreover, we also checked for the protein levels of these targets in HCT116-/- (with endogenous expression of Δ40p53), we observe that the abundance of SGSH, CDK11B and CDK5R1 was very high compared to HCT116+/+ **(Figure 5G)**. This observation was in line with Figure 3A, where miR-4671-5p levels were lower in HCT116-/- than in HCT116+/+. This contrasting regulation of miR-4671-5p and its targets mediated by the presence of Δ40p53 confirmed the involvement of these molecules in a single pathway.

To confirm the regulation of target mRNAs by Δ40p53, we partially silenced Δ40p53 in HCT116-/- and miR-4671-5p target mRNA expression mediated by siRNA. The results showed that SGSH, CDK11B and CDK5R1 mRNA expression significantly decreased under silenced Δ40p53 **(Figure 5H, I)**. These findings confirmed that Δ40p53 positively regulates SGSH, CDK11B, and CDK5R1 mRNA expression. The Δ40p53-mediated positive regulation of mRNAs was directed via downregulated miR-4671-5p expression **(Figure 2A)**. We overexpressed miR-4671-5p in HCT116 -/- cells to determine the direct effects of miRNAs on their targets. The expression of SGSH, CDK11B and CDK5R1 mRNAs was decreased **(Figure 5J, K)** and the effect was the most significant on SGSH mRNA.

Δ40p53 expression in colorectal cancer stratifies miR-4671-5p and *SGSH* levels

To extend our findings in colon cancer cell-line and to ascertain relevance of Δ40p53-related changes in miR-4671-5p and SGSH, we analysed a small cohort of colorectal cancer (CRC) patient samples available to us. Relevant clinical findings in this cohort are tabulated in **Figure S1, Table 1.** Processed tissue samples from the patients were interrogated for Δ40p53 protein expression **(Figure 6A)** and binned into Δ40p53-high (C4, C1, C14, C5) and Δ40p53-low (C8, C2, C3, C11, C15, C16) groups by densitometric analysis of immunoblots **(Figure 6B)**. C11 was excluded on account of near-absence of p53 as well as Δ40p53 expression relative to other CRC samples. Normalized expression of miR-4671-5p and *SGSH* mRNA levels from tumours revealed low miRNA and high mRNA levels in the Δ40p53-high compared to Δ40p53-low group **(Figure 6C-D)**, supporting our earlier findings in HCT116+/+ and -/- cells. Importantly, the levels of miR-4671-5p and *SGSH* were inversely correlated (Pearson r = -0.8061, two-tailed p-value =0.0087) in CRC patients as well **(Figure 6E)**.

Further, to analyse association of Δ40p53 in metastatic progression of CRC, we correlated its levels with TNM clinical classification of tumours that denotes anatomic extent of the disease as well as prognostic cancer staging. Here we observed that the samples with relatively high Δ40p53 (C1, C4, C5 and C14) had lymph node metastasis; histopathological analysis revealed normal appearing colonic mucosal glands in adjacent normal tissues **(Figure S2 A)**, whereas tumor sections obtained from the qualified tumour blocks show glandular pattern of adenocarcinoma enriched in pleomorphic cells with a vesicular nucleus with nucleoli surrounded by desmoplastic (fibrous) stroma and inflammatory cells . Relevantly, these samples (C1, C4, C5 and C14) demonstrate extensive tumour infiltration and deposits, indicating nodal metastasis and more advanced disease **(Figure S2 B)**, implying that Δ40p53 is associated with aggressive disease progression in CRC.

Cellular role of miR-4671-5p and target-mRNA interaction

Further, the direct binding experiment was performed using luciferase constructs to establish a direct link between miR-4671 and its targets. 3'UTRs of CDK5R1 and SGSH containing miR-4671 binding sites were cloned in luciferase constructs. Following this, mutations were generated in the 3'UTRs at miR-4671-5p binding sites **(Figure 7 A, B)**. HCT116-/- cells were transfected with CDK5R1 and SGSH 3'UTR WT and mutants in the background of miR-4671-5p overexpression. The overexpression of miR-4671-5p decreased the luciferase activity as compared to the control. Additionally, when the miR-4671-5p binding site was mutated in the 3'UTRs, the inhibitory effect on the luciferase was rescued, resulting in increased luciferase activity **(Figure 7 C, D).** This result suggests that miR-4671-5p directly binds to CDK5R1 and SGSH 3'UTRs, with more significant effect observed on SGSH.

As mentioned earlier **(Figure 5B-C)**, survival-correlated SGSH levels trend opposite to the levels of miR-4671-5p in certain cancer types, which suggests a direct possible link between the miRNA and the mRNA. However, the functional effect of mRNA is mainly mediated through its protein expression, therefore we checked the effect of siΔ40p53 or overexpression of miR-4671-5p on the respective protein levels. In both conditions, we observed a substantial and consistent reduction in SGSH protein levels reflecting the mRNA levels (**Figure 7 E, F**). This result suggested that SGSH mRNA could be a significant target downstream to Δ40p53-miR-4671-5p pathway. Finally, it was essential to decipher the direct role of miR-4671-5p on any cellular process. Since most of the selected targets of miR-4671-5p were directed toward cell cycle regulation, we checked for the changes in cell cycle phases

upon miR-4671-5p overexpression. We observed that the percentage of cells in the S phase were significantly increased, whereas the number of cells in the G2 phase decreased **(Figure 7G),** indicating the activation of a potential S-phase checkpoint which accumulated the cells in the S phase and prevented them from proceeding to G2. Thus, miR-4671-5p can regulate the cell cycle and possibly other associated cellular processes.

DISCUSSION

MicroRNAs regulate diverse cellular processes, including embryonic development, cell cycle, proliferation, and survival. Cancer is often associated with changes in miRNA expression [33]. Several studies have identified p53-regulated miRNAs and their roles in cancer [34]. Common malignancies express different p53 isoforms [6]. However, miRNA regulation by p53 isoforms had remained unknown until recently, and we showed that Δ40p53 specifically upregulates miR-186-5p and downregulates expression of the oncogene YY1, leading to a decrease in cell proliferation [22]. The function(s) of Δ40p53 has not been studied in detail, although its importance has been acknowledged given its roles in cellular functions such as apoptosis, cell cycle regulation, senescence, migration, and invasion [8]. If Δ40p53 is an important regulatory molecule, the pertinent question is which cellular pool of RNAs, specifically long non-coding (lnc) and microRNAs, are regulated. This has gained increasing importance in many areas of research.

Here, we identified several miRNAs of which their expression is regulated by Δ40p53, either differentially or to the same extent as p53. We then assessed the role of miR-4671-5p in cellular processes, as it was regulated exclusively by Δ40p53. Overexpressed Δ40p53 decreased, whereas p53 did not change expression of the novel miR-4671-5p. However, overexpressed 14A (combination of Δ40p53 and p53) decreased in miR-4671-5p expression, indicating that p53 facilitates the Δ40p53-mediated regulation of miR-4671-5p **(Figure 2B)**. Likewise, different ratios of p53 and Δ40p53 reduced miR-4671-5p under all conditions where both isoforms were present **(Figure 4D)**. This indicated that a differential abundance of p53 and Δ40p53 expression in cancer will accordingly lead to variable expression of downstream targets. To characterize the role of miR-4671-5p, we identified potential mRNA targets using bioinformatic analysis **(Figure S1, Table 2)** and selected a unique target, SGSH, that plays a metabolic role in governing cellular function. We report possible prognostic value of SGSH gene expression in certain tumor types **(Figure 5B-C)**; miR-4671-

5p levels trend oppositely in these cancer types **(Figure 4A)**. High SGSH expression was also significantly correlated with poor survival in glioblastoma multiforme (GBM), a highly malignant adult brain tumor **(Figure S1, Table 4)**. In addition, high hsa-miR-4671-5p is correlated with poor survival in a miRNA expression dataset in neuroblastoma, a common pediatric tumor, while low SGSH levels are significantly correlated with poor survival in multiple neuroblastoma gene expression datasets **(Figure S1, Table 4)**, providing further evidence of a putative link between the two. While the prognostic value of *SGSH* is significant, the seemingly confounding directionality in survival-correlation (high levels correlated to better survival in pancreatic adenocarcinoma and neuroblastoma versus low levels, in colon tumor and GBM) hints that SGSH is not a bona fide proto-oncogene or tumor suppressor; rather such differences may be explained by unique cancer-specific adaptation programs modifying Δ40p53-miR-4671-5p-SGSH axis that requires further investigation. Further, from enrichment analysis, we selected CDK11B and CDK5R1 as potential targets. We found that overexpressed Δ40p53 increased the abundance of all targets **(Figure 5D-F)**, the proteins also have a higher abundance in the presence of endogenous Δ40p53 **(Figure 5G)**. Although miR-4671-5p expression was decreased by co-expressed Δ40p53 and FLp53 **(Figure 4D)**, this trend was not apparent at the target mRNA level **(Figure 5D-F)**. This might stem from the activated or deactivated expression of other miRNA by combined p53 isoforms, which in turn would influence target mRNA regulation by miR-4671-5p. We then determined the relevance of the Δ40p53-miR4671-5p-mRNA axis. Target mRNA expression was directly decreased by overexpressed miRNA and silenced Δ40p53 **(Figure 5H and K)**, confirming a link between them. Analysis of an Indian cohort of colorectal carcinoma (CRC) patients pointed to the stratification of samples with both low miR-4671-5-p and high SGSH mRNA levels into the subgroup of patients where Δ40p53 expression was high **(Figure 6A-D**). Overall, miR-4671-5p and SGSH levels were inversely correlated in our cohort **(Figure 6E).** Additionally, TNM staging and histopathological staining from the patient samples showed high Δ40p53 (C1, C4, C5 and C14) in patients with lymph node metastasis, implying that high Δ40p53 is associated with more advanced CRC. Demographic and clinical profile of colorectal cancers in India differs from the western world, with higher incidence in younger patients, higher proportion of signet ring carcinomas, and advanced stage presentation and future comparative studies may be of clinical and mechanistic relevance[35]. For clinical settings, a neoepitope-like antibody may be developed leveraging potentially unique structural features of the N-terminus of Δ40p53 as a more advanced detection tool. Further,

Figure 7A-D shows mutant experiments with SGSH and CDK5R1 3'UTRs which established a direct link between miR-4671-5p and mRNAs. Our finding that Δ40p53, but not FLp53 regulated the miR-4671-5p–SGSH axis suggests the biological significance of Δ40p53 to metabolic regulation.

We measured protein levels of target mRNAs to determine the cellular effects of interactions. Direct miRNA overexpression and silenced Δ40p53 decreased SGSH protein levels **(Figure 7E, F)**. We assessed the physiological relevance of SGSH and miRNA interactions before delving into the cellular effects of this regulation. The SGSH encodes a sulfamidase enzyme associated with the lysosomal degradation of heparan sulfate, a glycosaminoglycan. Mutations in SGSH cause impaired degradation of heparan sulfate in MPS Type IIIA [36, 37]. How GAGs affect the cell cycle, a complex process that controls cell growth and division, in MPS disorders has been investigated. Flow cytometry findings have revealed disturbed cell cycle in all MPS types [38]. These findings suggest that SGSH is directly involved in cell cycle regulation. Along with SGSH, other targets of miR-4671-5p, namely CDK11B and CDK5R1are also associated with cell cycle regulation.

Therefore, we directly examined whether miR-4671-5p mediates cell cycle effects on different cell cycle phases. Upon miR-4671-5p overexpression, the ratios (%) of cells respectively increased and decreased in the S and G2 phases **(Figure 7G)**. The increased abundance of S-phase cells may be attributed to cell cycle arrest in the intra-S phase. While this is expected from regulation impinging on CDK5R1 and CDK11B, the effect of SGSH on cell cycle has been relatively obscure. Populations in the S and G2 phases are respectively increased and decreased in MPS Type IIIA, where SGSH is mutated [38]. Heparan sulfate inhibits topoisomerase 1 activity during DNA replication [39], and blocking this activity causes cell cycle arrest at the intra-S phase [40]. Thus, the inhibition of SGSH expression by miR-4671-5p, apart from inhibiting cell-cycle regulatory kinase functions, might increase the heparan sulfate content in cells, combinatorically causing an increase in S-phase cell counts (intra-S-phase arrest). Thus, Δ40p53 decreases miR-4671-5p expression, which leads to increased SGSH levels that help to maintain metabolic and cellular homeostasis **(Figure 8)**.

ACKNOWLEDGEMENTS

We are grateful to Prof. J.C. Bourdon, University of Dundee, UK and Dr. Robin Fahraeus, INSERM, France, for providing us with the anti-p53 antibody. We want to acknowledge

NIBMG (National Institute of Biomedical Genomics, Kalyani, WB, India) for providing an RNA sequencing facility. We also thank the present and past SD lab members for their helpful discussion of the work. A research grant supports this work to SD from the Department of Biotechnology (DBT), Govt. of India. SD also acknowledges the J.C. Bose fellowship for research support. The DBT-IISc partnership program also supported this study. DST Fund for Improvement of Science and Technology Infrastructure (FIST) level II infrastructure and University Grants Commission Centre of Advanced Studies support is acknowledged.

AUTHOR CONTRIBUTIONS

AP and SD: Conception and design of studies analysis, interpretation, and article writing. AP, SKT and PKG: performing experiments, interpretation of results and article editing. DK: bioinformatic analysis, interpretation of results, article writing and editing. SaG, SP and AM: RNA sequencing and analysis. SoG: Colorectal cancer sample collection and experimental procedures; PC: Patient recruitment; KMP: Histological analysis; MD: technical review and coordination for colorectal cancer samples. SD: Funding acquisition, supervision and project management.

DATA AVAILABILITY STATEMENT

The sequencing data files obtained is available in the online biorepository forum with the SRP BioProject ID **PRJEB47067.**

CONFLICT OF INTEREST

The authors declare no conflict of interest.

REFERENCE

1. Kops GJ, Weaver BA, Cleveland DW. On the road to cancer: aneuploidy and the mitotic checkpoint. *Nat Rev Cancer* 2005, **5**(10)**:** 773-785.

2. Powell DJ, Hrstka R, Candeias M, Bourougaa K, Vojtesek B, Fahraeus R. Stress-dependent changes in the properties of p53 complexes by the alternative translation product p53/47. *Cell Cycle* 2008, **7**(7)**:** 950-959.

512 3. Rivlin N, Brosh R, Oren M, Rotter V. Mutations in the p53 Tumor Suppressor Gene:
513 Important Milestones at the Various Steps of Tumorigenesis. *Genes Cancer* 2011, **2**(4)**:** 466-
514 474.

515
516 4. Bourdon JC. p53 and its isoforms in cancer. *Br J Cancer* 2007, **97**(3)**:** 277-282.

517
518 5. Khoury MP, Bourdon JC. p53 Isoforms: An Intracellular Microprocessor? *Genes Cancer* 2011,
519 **2**(4)**:** 453-465.

520
521 6. Vieler M, Sanyal S. p53 Isoforms and Their Implications in Cancer. *Cancers (Basel)* 2018,
522 **10**(9).

523
524 7. Bourdon JC, Fernandes K, Murray-Zmijewski F, Liu G, Diot A, Xirodimas DP*, et al.* p53
525 isoforms can regulate p53 transcriptional activity. *Genes Dev* 2005, **19**(18)**:** 2122-2137.

526
527 8. Steffens Reinhardt L, Zhang X, Wawruszak A, Groen K, De Iuliis GN, Avery-Kiejda KA. Good
528 Cop, Bad Cop: Defining the Roles of Delta40p53 in Cancer and Aging. *Cancers (Basel)* 2020,
529 **12**(6).

530
531 9. Ray PS, Grover R, Das S. Two internal ribosome entry sites mediate the translation of p53
532 isoforms. *EMBO Rep* 2006, **7**(4)**:** 404-410.

533
534 10. Khan D, Katoch A, Das A, Sharathchandra A, Lal R, Roy P*, et al.* Reversible induction of
535 translational isoforms of p53 in glucose deprivation. *Cell Death Differ* 2015, **22**(7)**:** 1203-
536 1218.

537
538 11. Sharathchandra A, Katoch A, Das S. IRES mediated translational regulation of p53 isoforms.
539 *Wiley Interdiscip Rev RNA* 2014, **5**(1)**:** 131-139.

540
541 12. Ghosh A, Stewart D, Matlashewski G. Regulation of human p53 activity and cell localization
542 by alternative splicing. *Mol Cell Biol* 2004, **24**(18)**:** 7987-7997.

543
544 13. Hafsi H, Santos-Silva D, Courtois-Cox S, Hainaut P. Effects of Delta40p53, an isoform of p53
545 lacking the N-terminus, on transactivation capacity of the tumor suppressor protein p53.
546 *BMC Cancer* 2013, **13:** 134.

547
548 14. Ohki R, Kawase T, Ohta T, Ichikawa H, Taya Y. Dissecting functional roles of p53 N-terminal
549 transactivation domains by microarray expression analysis. *Cancer Sci* 2007, **98**(2)**:** 189-200.

550
551 15. Ota A, Nakao H, Sawada Y, Karnan S, Wahiduzzaman M, Inoue T*, et al.* Delta40p53alpha
552 suppresses tumor cell proliferation and induces cellular senescence in hepatocellular
553 carcinoma cells. *J Cell Sci* 2017, **130**(3)**:** 614-625.

16. Maier B, Gluba W, Bernier B, Turner T, Mohammad K, Guise T*, et al.* Modulation of mammalian life span by the short isoform of p53. *Genes Dev* 2004, **18**(3)**:** 306-319.

17. Bourougaa K, Naski N, Boularan C, Mlynarczyk C, Candeias MM, Marullo S*, et al.* Endoplasmic reticulum stress induces G2 cell-cycle arrest via mRNA translation of the p53 isoform p53/47. *Mol Cell* 2010, **38**(1)**:** 78-88.

18. Thomas SE, Malzer E, Ordonez A, Dalton LE, van TWEFA, Liniker E*, et al.* p53 and translation attenuation regulate distinct cell cycle checkpoints during endoplasmic reticulum (ER) stress. *J Biol Chem* 2013, **288**(11)**:** 7606-7617.

19. Ungewitter E, Scrable H. Delta40p53 controls the switch from pluripotency to differentiation by regulating IGF signaling in ESCs. *Genes Dev* 2010, **24**(21)**:** 2408-2419.

20. Hinault C, Kawamori D, Liew CW, Maier B, Hu J, Keller SR*, et al.* Delta40 Isoform of p53 controls beta-cell proliferation and glucose homeostasis in mice. *Diabetes* 2011, **60**(4)**:** 1210-1222.

21. Zhang X, Groen K, Morten BC, Steffens Reinhardt L, Campbell HG, Braithwaite AW*, et al.* Effect of p53 and its N-terminally truncated isoform, Delta40p53, on breast cancer migration and invasion. *Mol Oncol* 2022, **16**(2)**:** 447-465.

22. Katoch A, Tripathi SK, Pal A, Das S. Regulation of miR-186-YY1 axis by the p53 translational isoform Δ40p53: implications in cell proliferation. *Cell Cycle* 2021, **20**(5-6)**:** 561-574.

23. Pal A, Ghosh PK, Das S. The "LINC" between Δ40p53-miRNA Axis in the Regulation of Cellular Homeostasis. *Mol Cell Biol* 2023, **43**(7)**:** 335-353.

24. Sun Y, Manceau A, Frydman L, Cappuccio L, Neves D, Basso V*, et al.* Delta40p53 isoform up-regulates netrin-1/UNC5B expression and potentiates netrin-1 pro-oncogenic activity. *Proc Natl Acad Sci U S A* 2021, **118**(36).

25. Xu F, Wang Y, Ling Y, Zhou C, Wang H, Teschendorff AE*, et al.* dbDEMC 3.0: Functional Exploration of Differentially Expressed miRNAs in Cancers of Human and Model Organisms. *Genomics, Proteomics & Bioinformatics* 2022.

26. Agarwal V, Bell GW, Nam J-W, Bartel DP. Predicting effective microRNA target sites in mammalian mRNAs. *eLife* 2015, **4:** e05005.

27. Chen Y, Wang X. miRDB: an online database for prediction of functional microRNA targets. *Nucleic Acids Res* 2020, **48**(D1)**:** D127-d131.

28. Liu W, Wang X. Prediction of functional microRNA targets by integrative modeling of microRNA binding and target expression data. *Genome Biology* 2019, **20**(1)**:** 18.

29. Zhang L, Liao Y, Tang L. MicroRNA-34 family: a potential tumor suppressor and therapeutic candidate in cancer. *Journal of Experimental & Clinical Cancer Research* 2019, **38**(1)**:** 53.

30. Li X, Xiao R, Chen B, Yang G, Zhang X, Fu Z*, et al.* A novel mutation of SGSH and clinical features analysis of mucopolysaccharidosis type IIIA. *Medicine* 2018, **97**(52)**:** e13758.

31. Anuraga G, Lang J, Xuan DTM, Ta HDK, Jiang JZ, Sun Z*, et al.* Integrated bioinformatics approaches to investigate alterations in transcriptomic profiles of monkeypox infected human cell line model. *Journal of infection and public health* 2024, **17**(1)**:** 60-69.

32. Ye J, Liu P, Li R, Liu H, Pei W, Ma C*, et al.* Biomarkers of connective tissue disease-associated interstitial lung disease in bronchoalveolar lavage fluid: A label-free mass spectrometry-based relative quantification study. *Journal of clinical laboratory analysis* 2022, **36**(5)**:** e24367.

33. Israel A, Sharan R, Ruppin E, Galun E. Increased MicroRNA Activity in Human Cancers. *PLOS ONE* 2009, **4**(6)**:** e6045.

34. Takwi A, Li Y. The p53 Pathway Encounters the MicroRNA World. *Current genomics* 2009, **10**(3)**:** 194-197.

35. Patil PS, Saklani A, Gambhire P, Mehta S, Engineer R, De'Souza A*, et al.* Colorectal Cancer in India: An Audit from a Tertiary Center in a Low Prevalence Area. *Indian journal of surgical oncology* 2017, **8**(4)**:** 484-490.

36. Griffin LS, Gloster TM. The Enzymatic Degradation of Heparan Sulfate. *Protein and peptide letters* 2017, **24**(8)**:** 710-722.

37. Boado RJ, Lu JZ, Hui EK-W, Pardridge WM. Reduction in Brain Heparan Sulfate with Systemic Administration of an IgG Trojan Horse–Sulfamidase Fusion Protein in the Mucopolysaccharidosis Type IIIA Mouse. *Molecular Pharmaceutics* 2018, **15**(2)**:** 602-608.

38. Brokowska J, Gaffke L, Pierzynowska K, Cyske Z, Węgrzyn G. Cell cycle disturbances in mucopolysaccharidoses: Transcriptomic and experimental studies on cellular models. *Experimental biology and medicine (Maywood, NJ)* 2022, **247**(18)**:** 1639-1649.

39. Kovalszky I, Dudás J, Oláh-Nagy J, Pogány G, Töváry J, Timár J*, et al.* Inhibition of DNA topoisomerase I activity by heparan sulfate and modulation by basic fibroblast growth factor. *Mol Cell Biochem* 1998, **183**(1-2)**:** 11-23.

40. Lin R-W, Yang C-N, Ku S, Ho C-J, Huang S-B, Yang M-C, *et al.* CFS-1686 Causes Cell Cycle Arrest at Intra-S Phase by Interference of Interaction of Topoisomerase 1 with DNA. *PLOS ONE* 2014, **9**(12): e113832.

FIGURE LEGENDS

Figure 1. Regulation of miRNA expression by p53 and its isoform Δ40p53

(A) Schematic of constructs used in study (B) Experimental setup prior to RNA sequencing. (C) Western blot analysis of cell extracts from H1299 cells expressing control, p53 only, Δ40p53 only and 14A construct, probed with CM1 after 48 h. (D) The cluster of differentially expressed miRNAs obtained from the small RNA sequencing data set. (E) The compressed cluster of significant differentially expressed miRNAs with p-value $\leq$ 0.05 (generated using Heatmapper).

Figure 2. Selection and validation of miRNAs for further studies

(A) Western blot analysis of cell extracts from H1299 cells expressing control, p53 only, Δ40p53 only and 14A construct, probed with CM1 after 48 h. (B-E) Quantitative PCR for validation of miR-4671-5p, miR-34a-5p, miR-548ae-5p, miR-301b-5p, respectively, in H1299 cells expressing control, p53 only, Δ40p53 only and 14A construct. (F) Table for comparative analysis of fold changes obtained in sequencing versus validation result. The criterion for statistical significance was $p \leq 0.05$ (*) or $p \leq 0.01$ (**) or $p \leq 0.001$(***)

Figure 3. Regulation of miRNAs by Δ40p53 and p53

(A) Western blot analysis of cell extracts from HCT116+/+ and HCT116-/-cells probed with CM1. (B) Quantitative PCR for validations of miR-4671-5p, miR-34a-5p and miR-548ae-5p in HCT116+/+ and HCT116-/-cells. (C) Quantitative PCR of miR-4671-5p, miR-34a-5p and miR-548ae-5p in HCT116+/+ cells transfected with si p53 (30nM) and non-specific si (si Nsp). (D) Western blot analysis of cell extracts from HCT116+/+ cells transfected with either si p53 (30nM) and non-specific si (si Nsp), probed with CM1. (E) Quantitative PCR of miR-4671-5p, miR-34a-5p and miR-548ae-5p in HCT116-/- cells transfected with si Δ40p53 (30nM) and non-specific si (si Nsp). (F) Western blot analysis of cell extracts from HCT116-

/- cells transfected with si∆40p53 (30nM) and non-specific si (si Nsp), probed with CM1. The criterion for statistical significance was $p \leq 0.05$ (*) or $p \leq 0.01$ (**) or $p \leq 0.001$(***)

Figure 4. Regulation of miRNAs by different ratios of ∆40p53 and p53

(A) Differential expression Profile of miRNAs in cancer vs. normal obtained from dbDEMC 3.0 database. (B) Western blot analysis of cell extracts from H1299 transfected cells with different ratios of p53 and ∆40p53 probed with CM1. (C-D) Quantitative PCR of miR-34a-5p and miR-4671-5p respectively in H1299 transfected with different ratios of p53 and ∆40p53. The criterion for statistical significance was $p \leq 0.05$ (*) or $p \leq 0.01$ (**) or $p \leq 0.001$(***).

Figure 5. Effect of ∆40p53-miR-4671-5p on the downstream mRNAs

(A) Table for miR-4671-5p targets selected in the study. (B-C) Kaplan-Meier estimates of survival for pancreatic adenocarcinoma (B) and colon tumor (C) classified by SGSH mRNA expression levels. The number of patients at risk is indicated for time increments of 12 or 24 months. p values were calculated using a log rank test. (D-F) Quantitative PCR of mRNA targets (SGSH, CDK11B and CDK5R1) in H1299 transfected cells with different ratios of p53 and ∆40p53. (G) Western blot analysis of cell extracts from HCT116+/+ and HCT116-/- cells probed with CM1, SGSH, CDK11B, CDK5R1 antibodies. (H) Quantitative PCR of SGSH, CDK11B and CDK5R1 in HCT116-/- cells transfected with si ∆40p53 (30nM) and non-specific si (si Nsp). (I) Western blot analysis of cell extracts from HCT116-/- cells transfected with si∆40p53 (30nM) and non-specific si (si Nsp), probed with CM1. (J) Quantitative PCR of miR-4671-5p in HCT116-/- cells transfected with miR-4671-5p overexpression construct. (K) Quantitative PCR of SGSH, CDK11B and CDK5R1 in HCT116-/- cells transfected with miR-4671-5p overexpression construct. The criterion for statistical significance was $p \leq 0.05$ (*) or $p \leq 0.01$ (**) or $p \leq 0.001$(***).

Figure 6: ∆40p53 expression level in colorectal cancer (CRC) patients stratifies miR-4671-5p and SGSH levels

(A) Western blot analysis of p53 and ∆40p53 protein expressions in fresh frozen resected tissue samples from CRC patients (C1-C5, C8, C11, C14-16). Western blots from HCT116+/+ (expresses both isoforms) and HCT116-/- (expresses only ∆40p53) colon cancer cells as markers for relative migration of p53 and ∆40p53 done in same gel and same membrane as C1-C5, at lower exposure than C1-C5. (B) Densitometric analysis of ∆40p53 band in CRC patients (arb. unit: arbitrary units), p-value from unpaired t-test (C) Quantitative

PCR Ct value of miR-4671-5p levels normalized to U6 RNA, p-value from unpaired t-test (D) Quantitative PCR Ct value of SGSH levels normalized to ACTB RNA, p-value from unpaired t-test. (E) Correlation of normalized miR-4671-5p Ct values with normalized SGSH Ct values across CRC patients. Simple linear regression line in grey (R^2=0.6498).

Figure 7: The cellular implications of miRNA-mRNA interaction

(A, B) Schematic of the mutation generated in the CDK5R1 3'UTR WT and SGSH 3'UTR WT in the miR-4671-5p binding site. (C, D) The effects of miR-4671-5p overexpression on the activity of wild□type and mutant 3'□UTRs of CDK5R1 and SGSH (respectively) were analyzed by luciferase reporter assay 48h post-transfection. (E) Western blot analysis of cell extracts from HCT116-/- cells transfected with siΔ40p53 (30nM) and non-specific si (si Nsp), probed with CM1 and SGSH. (F) Western blot analysis of cell extracts from HCT116-/- cells transfected with miR-4671-5p overexpression construct, probed with SGSH. (G) Analysis of different cell cycle phases of fixed cell extracts from HCT116-/- cells transfected with miR-4671-5p overexpression construct. The criterion for statistical significance was $p \leq 0.05$ (*) or $p \leq 0.01$ (**) or $p \leq 0.001$(***).

Figure 8: Model depicting the regulation of Δ40p53 mediated regulation of miR-4671-5p and their impact on cell cycle

(A) In the absence of Δ40p53, miR-4671-5p levels do not decrease, leading to increased target mRNA degradation. The residual mRNAs give rise to decreased proteins (e.g. SGSH), leading to Intra-S phase cell cycle arrest. The mechanism of arrest could be due to impaired degradation of Heparan Sulphate (HS) by SGSH, causing HS accumulation, thereby destabilizing the metabolic and cellular homeostasis. (B) However, when Δ40p53 is present, it decreases miR-4671-5p levels, preventing target mRNA degradation. The increase in residual mRNAs gives rise to more proteins (e.g., SGSH), which allows regular cell cycle propagation. Here the mechanism could be increased degradation of HS, which helps to stabilize the metabolic and cellular homeostasis.

Figure S1: (Table 1): Clinical and pathological details of the patient samples. *T, size and extent of the main tumor; N, number of nearby lymph nodes that have cancer; M, metastasis. **(Table 2)**: miR-4671-5p targets obtained from TargetScan 7.2 database and miRDB. **(Table 3)**: Result of PANTHER Statistical Overrepresentation Test of "GO molecular function"-terms obtained from 786 predicted miR-4671-5p targets, using all *Homo sapiens* genes as reference list. FDR: False Discovery Rate. Results for FDR $P < 0.05$ reported. **(Table 4)**: Survival analysis of patients as classified by SGSH mRNA expression levels in pancreatic adenocarcinoma, colon tumor, glioblastoma and neuroblastoma gene expression datasets available on R2: Genomics Analysis and Visualization Platform. p-values <0.07 reported, below 0.05 considered significant. Similar analysis for hsa-miR-4671-5p expression, as available in the sole miRNA expression dataset on R2.

Figure S2: (A) H&E images of FFPE samples from tumor and adjacent normal tissues. (Yellow arrow indicates tumor features) (B) H&E images of FFPE samples from lymph nodes with metastasized and normal lymph node tissues (Yellow arrow indicates deposited tumor cells)

Figure 1

A.

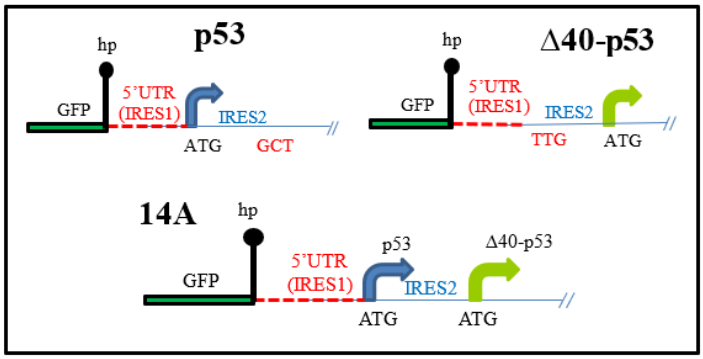

B. *WORK FLOW*

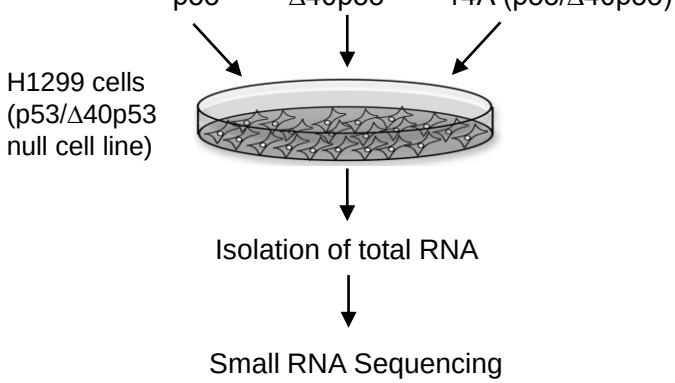

C.

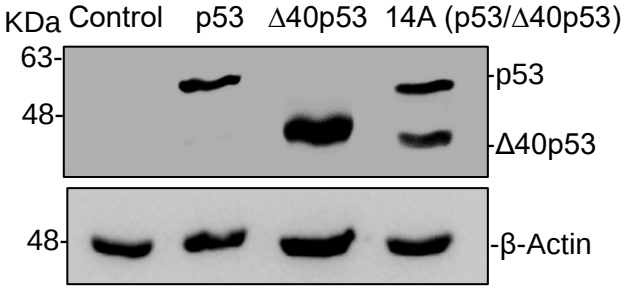

D.

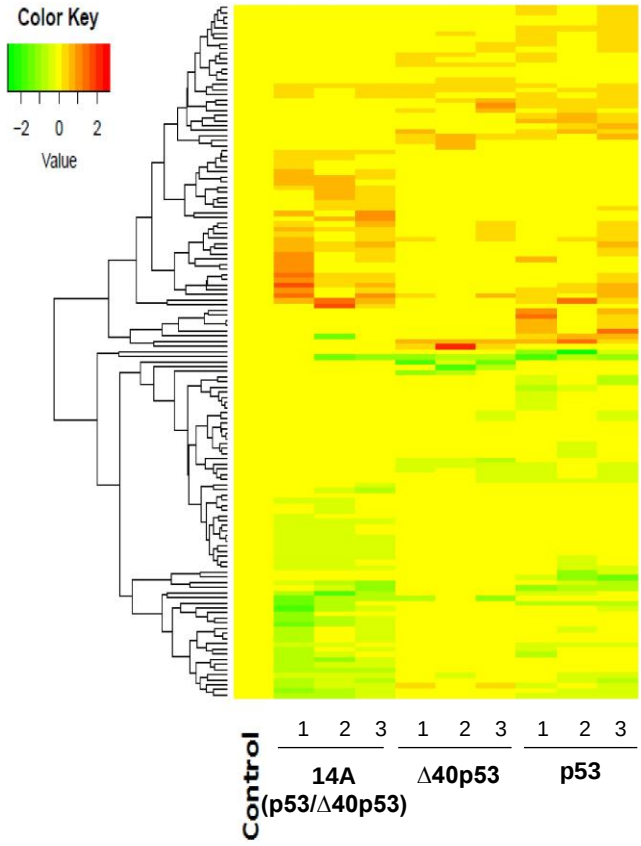

E.

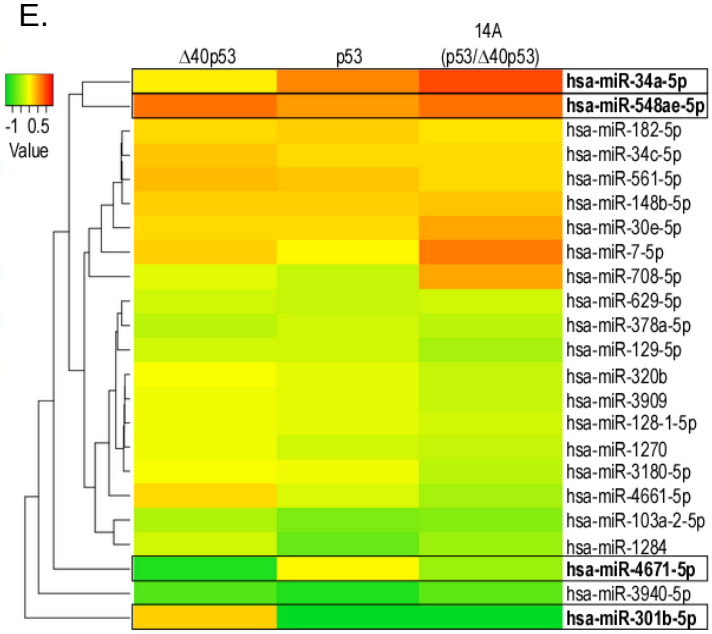

Figure 2

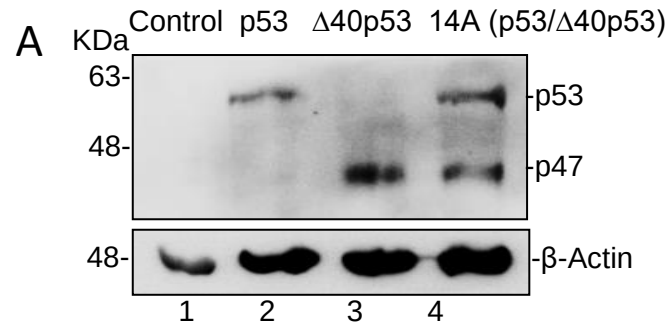

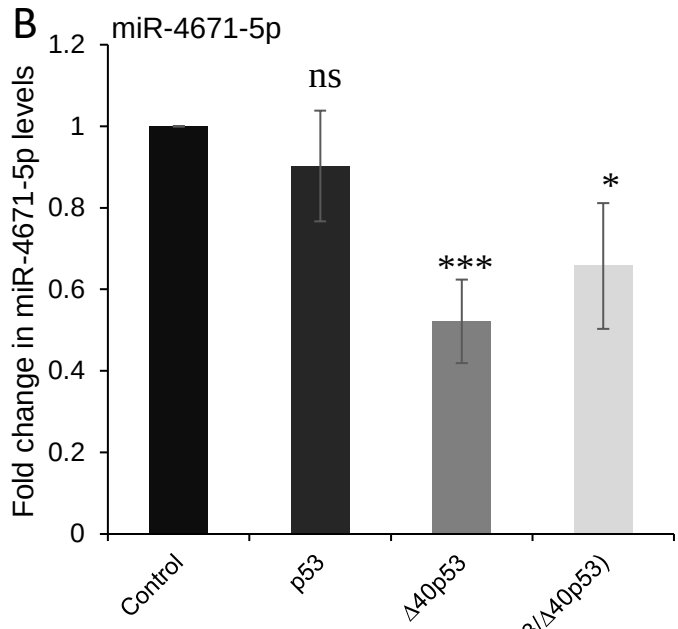

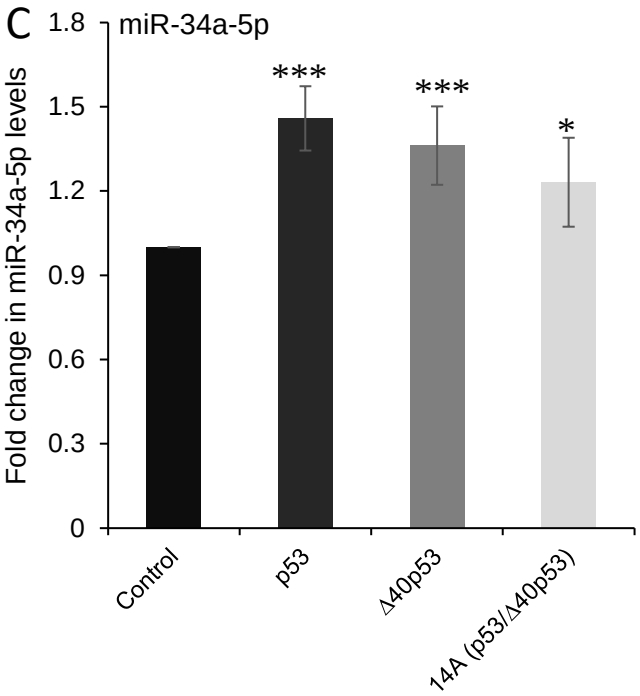

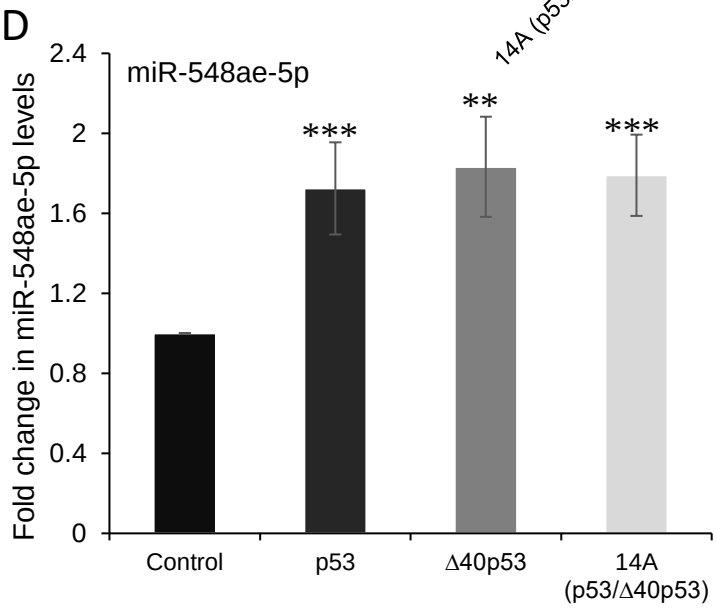

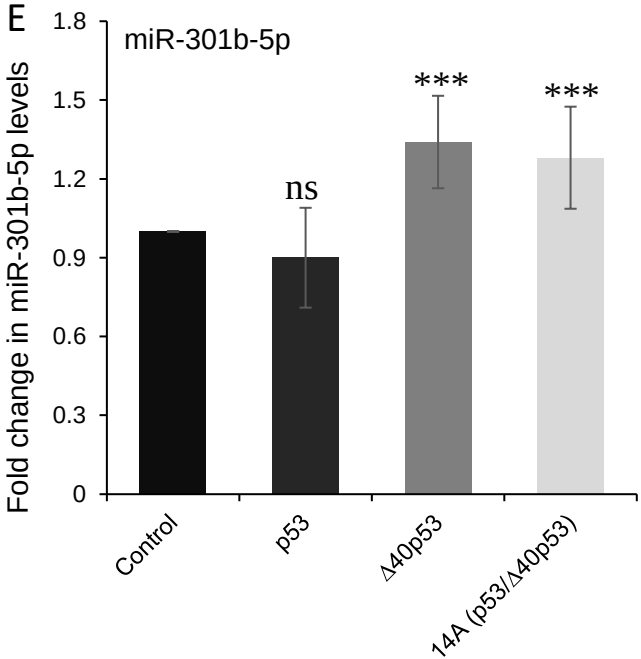

F

miRNAs	Condition	Sequencing Results	Validation
miR-4671-5p	p53	↑	NS
	Δ40p53	↓	↓
	14A	↓	↓
miR-34a-5p	p53	↑	↑
	Δ40p53	↑	↑
	14A	↑	↑
miR-548ae-5p	p53	↑	↑
	Δ40p53	↑	↑
	14A	↑	↑
miR-301b-5p	p53	↓	NS
	Δ40p53	↑	↑
	14A	↓	↑

Figure 3

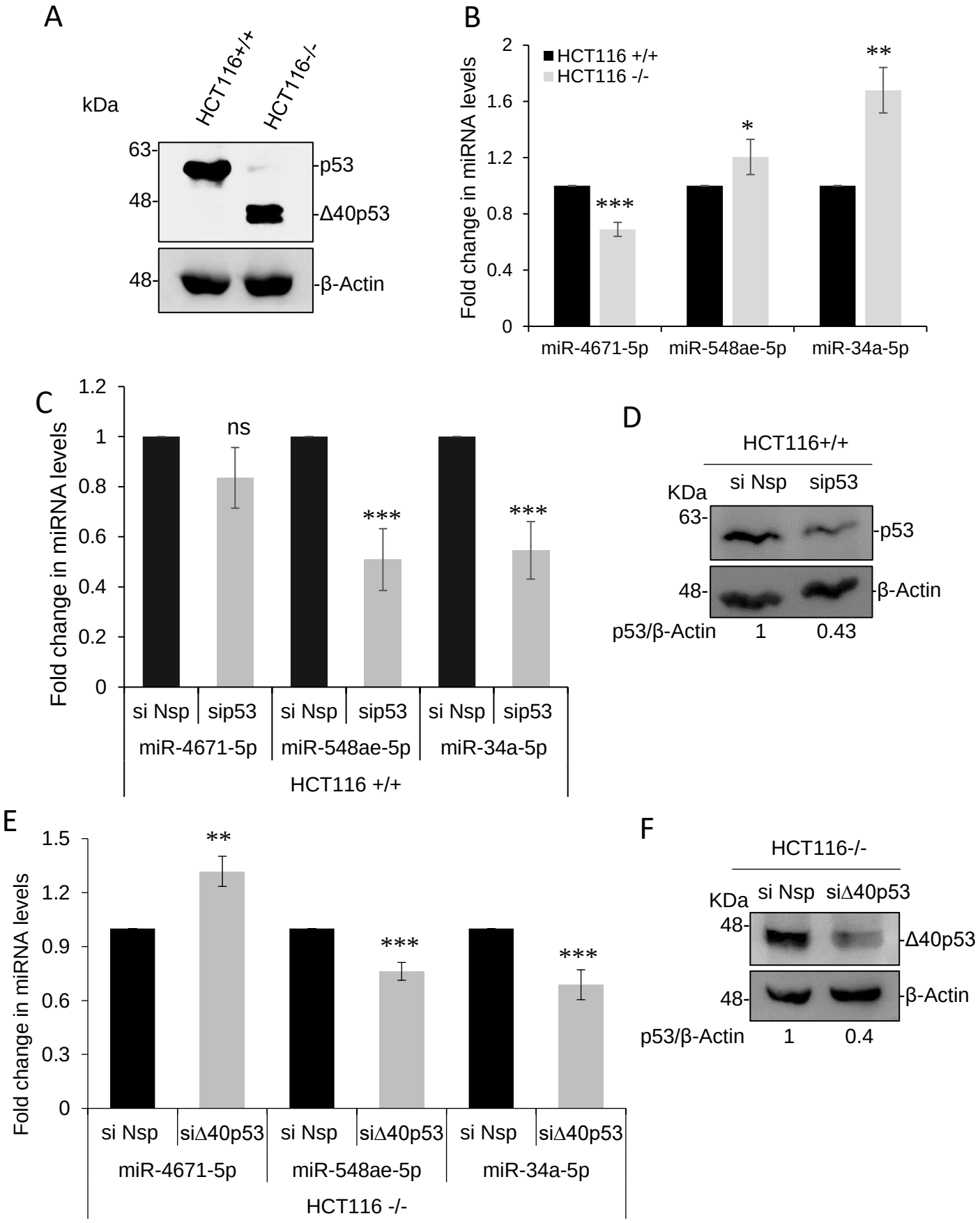
A
kDa
HCT116+/+
HCT116-/-
63-
48-
p53
Δ40p53
48-
β-Actin
B
HCT116 +/+
HCT116 -/-
Fold change in miRNA levels
2
1.6
1.2
0.8
0.4
0
***
*
**
miR-4671-5p
miR-548ae-5p
miR-34a-5p
C
Fold change in miRNA levels
1.2
1
0.8
0.6
0.4
0.2
0
ns
***
***
si Nsp
sip53
si Nsp
sip53
si Nsp
sip53
miR-4671-5p
miR-548ae-5p
miR-34a-5p
HCT116 +/+
D
HCT116+/+
si Nsp
sip53
KDa
63-
48-
p53
β-Actin
p53/β-Actin
1
0.43
E
Fold change in miRNA levels
1.5
1.2
0.9
0.6
0.3
0
**
***
***
si Nsp
siΔ40p53
si Nsp
siΔ40p53
si Nsp
siΔ40p53
miR-4671-5p
miR-548ae-5p
miR-34a-5p
HCT116 -/-
F
HCT116-/-
si Nsp
siΔ40p53
KDa
48-
48-
Δ40p53
β-Actin
p53/β-Actin
1
0.4

Figure 4

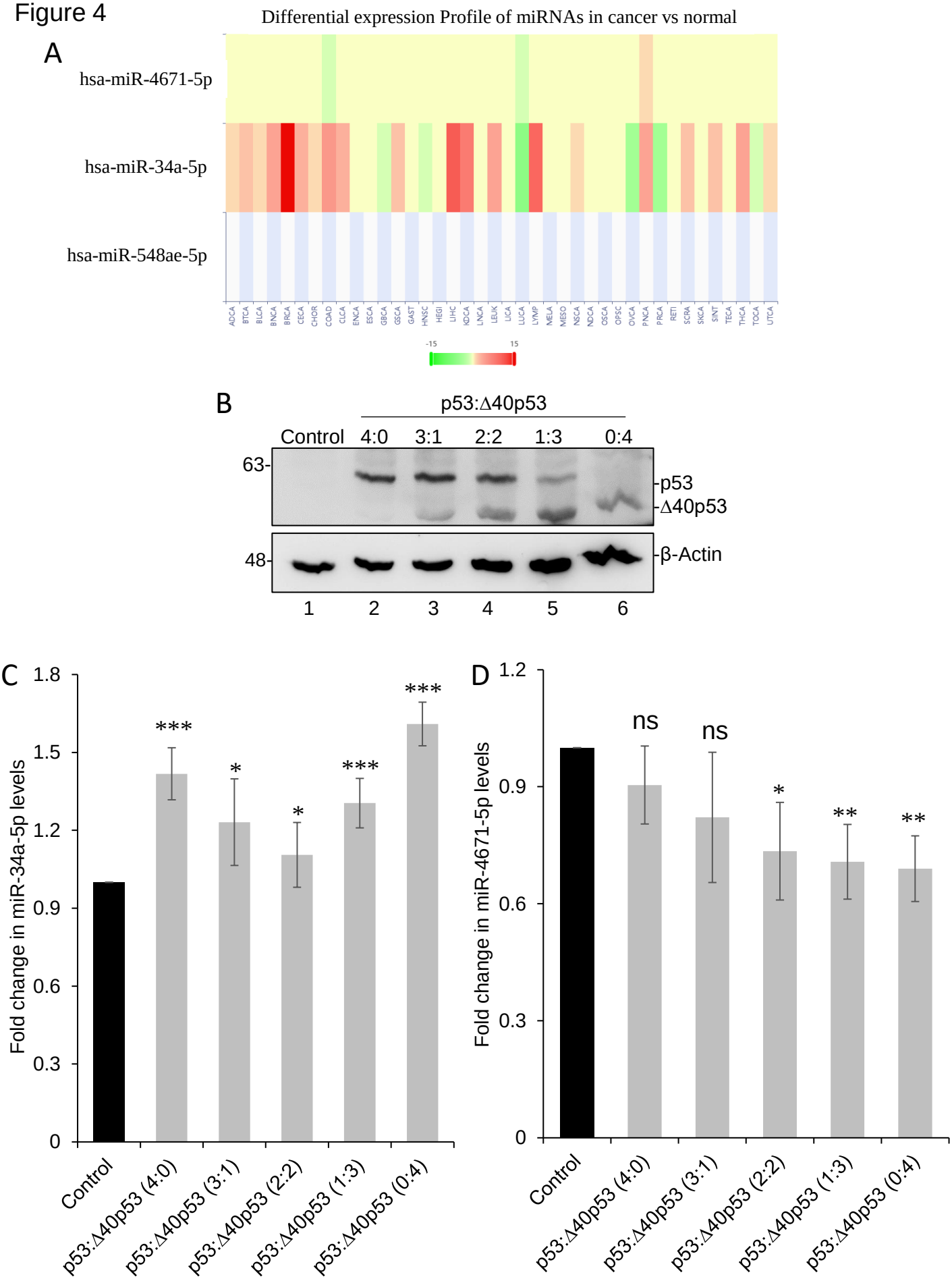
A
Differential expression Profile of miRNAs in cancer vs normal
hsa-miR-4671-5p
hsa-miR-34a-5p
hsa-miR-548ae-5p
ADCA BTCA BLCA BNCA BRCA CECA CHOR COAD CLCA ENCA ESCA GBCA GSCA GAST HNSC HEGI LIHC KDCA LNCA LEUK LICA LUCA LYMP MELA MESO NSCA NDCA OSCA OPSC OVCA PNCA PRCA RETI SCRA SKCA SINT TECA THCA TOCA UTCA
-15
15
B
p53:Δ40p53
Control 4:0 3:1 2:2 1:3 0:4
63-
48-
p53
Δ40p53
β-Actin
1 2 3 4 5 6
C
Fold change in miR-34a-5p levels
1.8
1.5
1.2
0.9
0.6
0.3
0
***
*
*
***
***
Control
p53:Δ40p53 (4:0)
p53:Δ40p53 (3:1)
p53:Δ40p53 (2:2)
p53:Δ40p53 (1:3)
p53:Δ40p53 (0:4)
D
Fold change in miR-4671-5p levels
1.2
0.9
0.6
0.3
0
ns
ns
*
**
**
Control
p53:Δ40p53 (4:0)
p53:Δ40p53 (3:1)
p53:Δ40p53 (2:2)
p53:Δ40p53 (1:3)
p53:Δ40p53 (0:4)

Figure 5

A

miRNA	Target	Function
miR-4671-5p	CDK5R1	Cell growth
	CDK11B	
	SGSH	Cell Metabolism/ Cell cycle

B

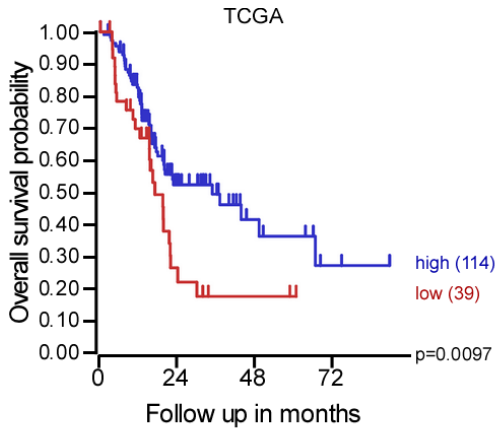

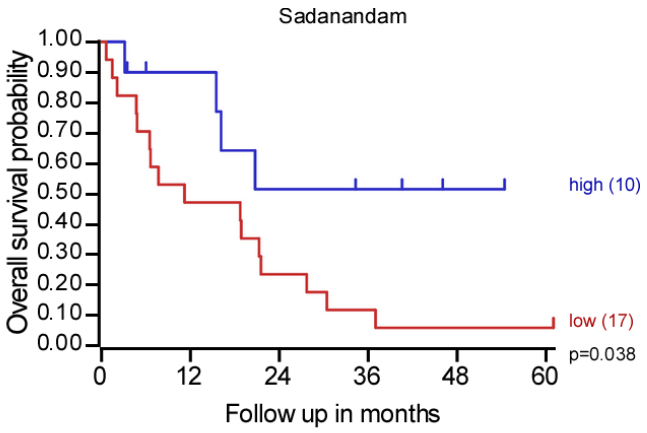

C

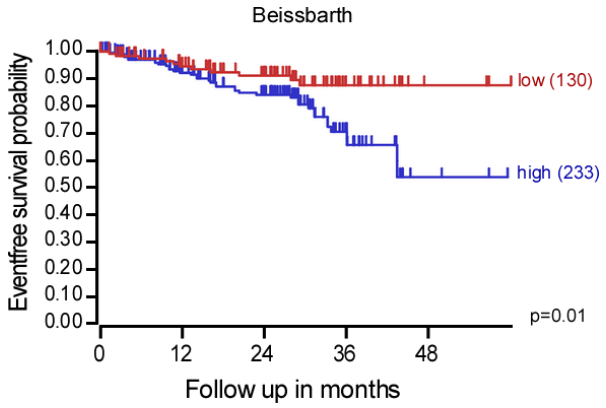

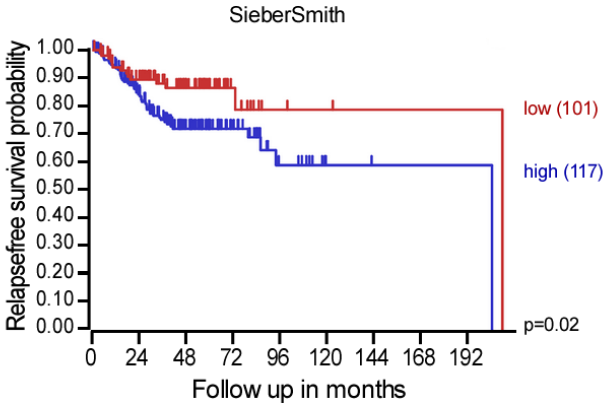

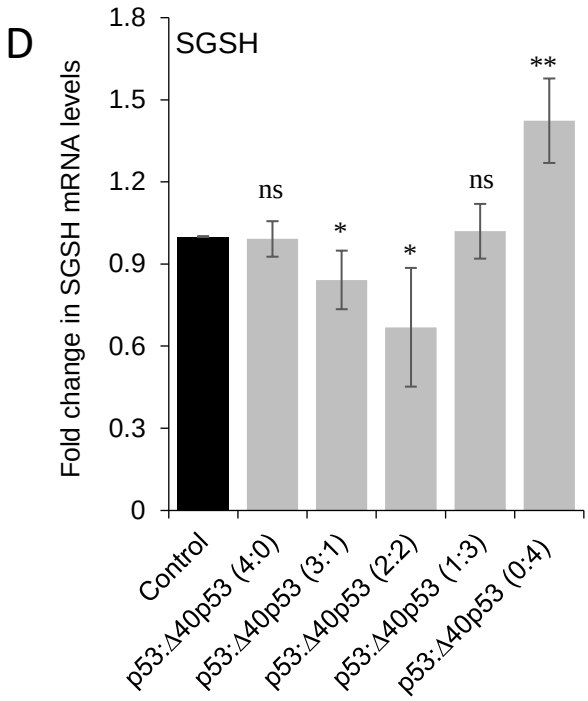
D
SGSH
Fold change in SGSH mRNA levels
1.8
1.5
1.2
0.9
0.6
0.3
0
ns
*
*
ns
**
Control
p53:Δ40p53 (4:0)
p53:Δ40p53 (3:1)
p53:Δ40p53 (2:2)
p53:Δ40p53 (1:3)
p53:Δ40p53 (0:4)

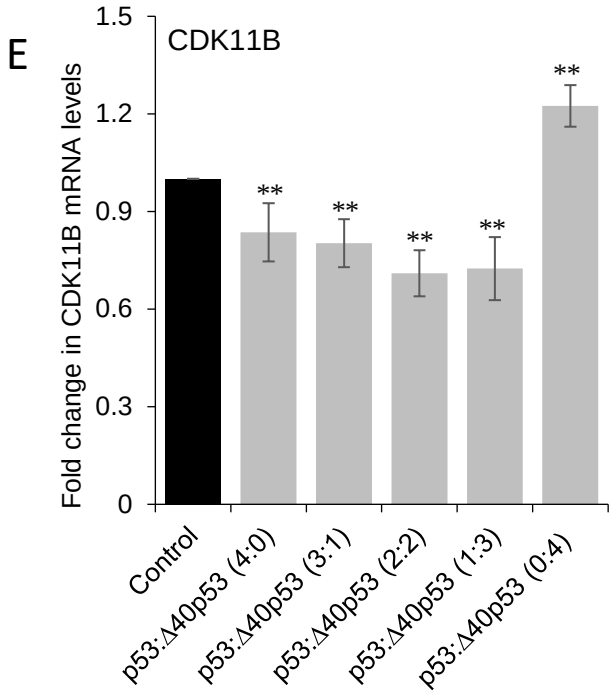
E
CDK11B
Fold change in CDK11B mRNA levels
1.5
1.2
0.9
0.6
0.3
0
**
**
**
**
**
Control
p53:Δ40p53 (4:0)
p53:Δ40p53 (3:1)
p53:Δ40p53 (2:2)
p53:Δ40p53 (1:3)
p53:Δ40p53 (0:4)

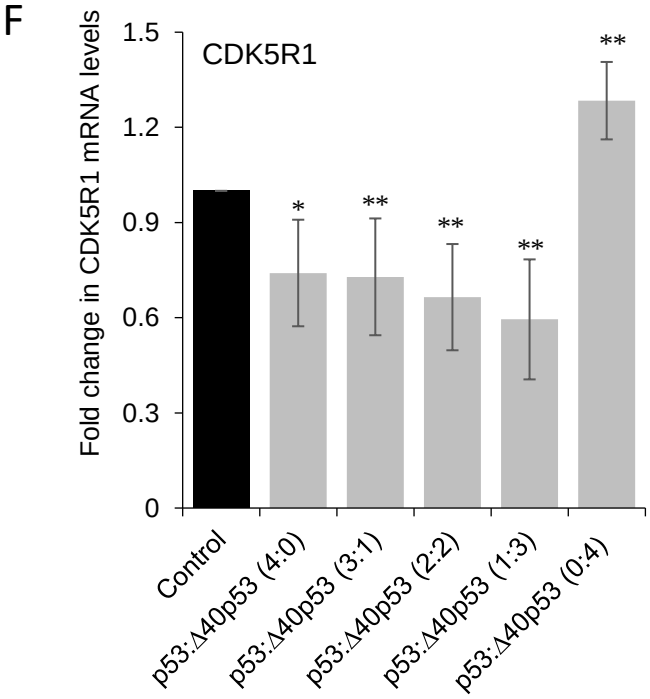
F
CDK5R1
Fold change in CDK5R1 mRNA levels
1.5
1.2
0.9
0.6
0.3
0
*
**
**
**
**
Control
p53:Δ40p53 (4:0)
p53:Δ40p53 (3:1)
p53:Δ40p53 (2:2)
p53:Δ40p53 (1:3)
p53:Δ40p53 (0:4)

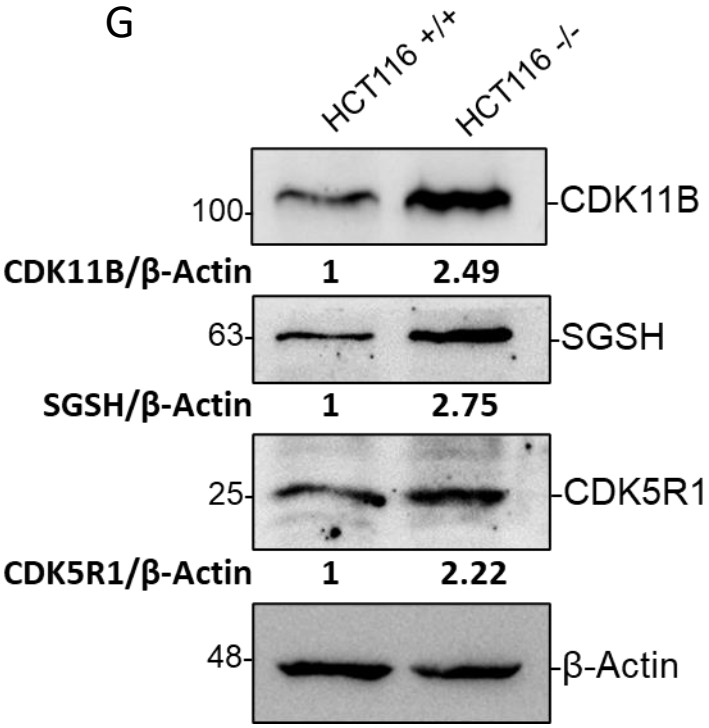
G
HCT116 +/+
HCT116 -/-
100
CDK11B
CDK11B/β-Actin
1
2.49
63
SGSH
SGSH/β-Actin
1
2.75
25
CDK5R1
CDK5R1/β-Actin
1
2.22
48
β-Actin

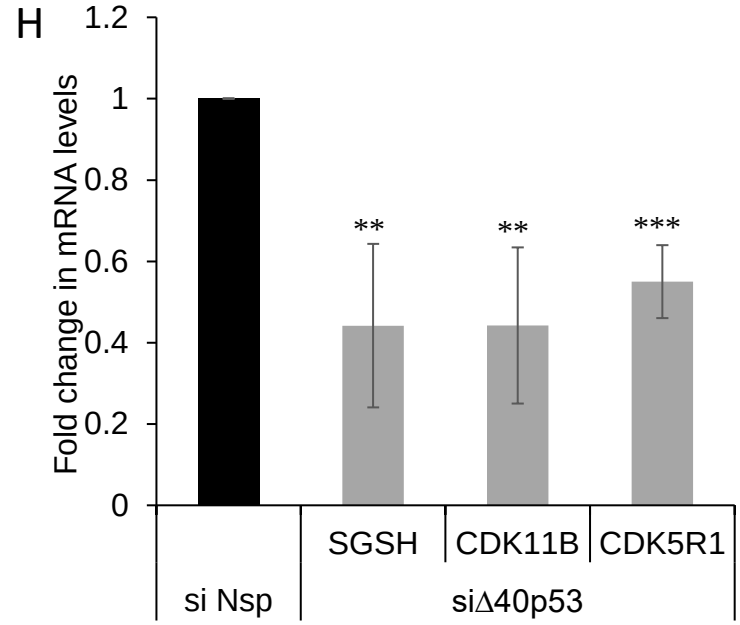
H
Fold change in mRNA levels
1.2
1
0.8
0.6
0.4
0.2
0
**
**
***
SGSH
CDK11B
CDK5R1
si Nsp
siΔ40p53

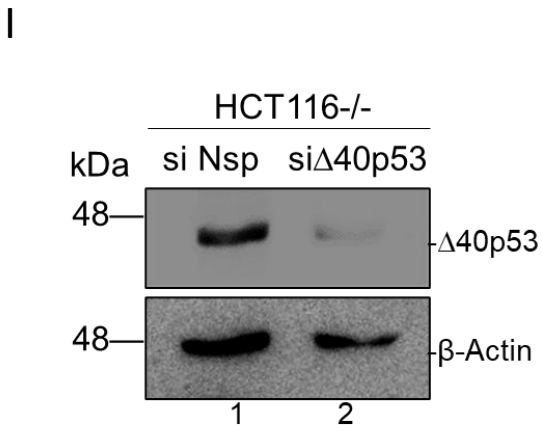
I
HCT116-/-
kDa
si Nsp
siΔ40p53
48
48
Δ40p53
β-Actin
1
2

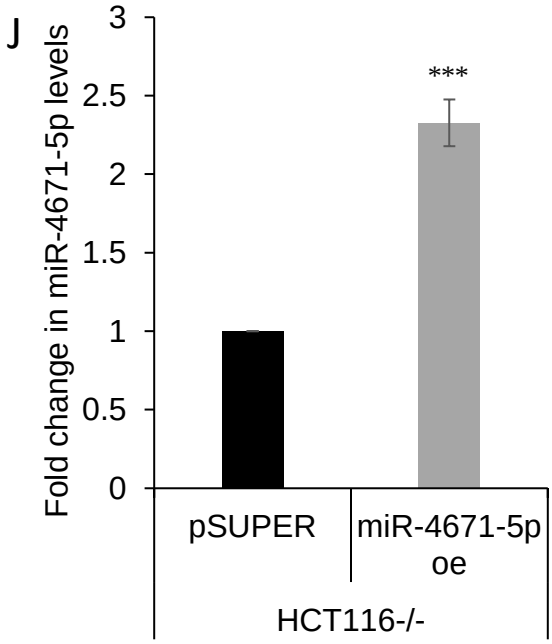
J
Fold change in miR-4671-5p levels
3
2.5
2
1.5
1
0.5
0
***
pSUPER
miR-4671-5p oe
HCT116-/-

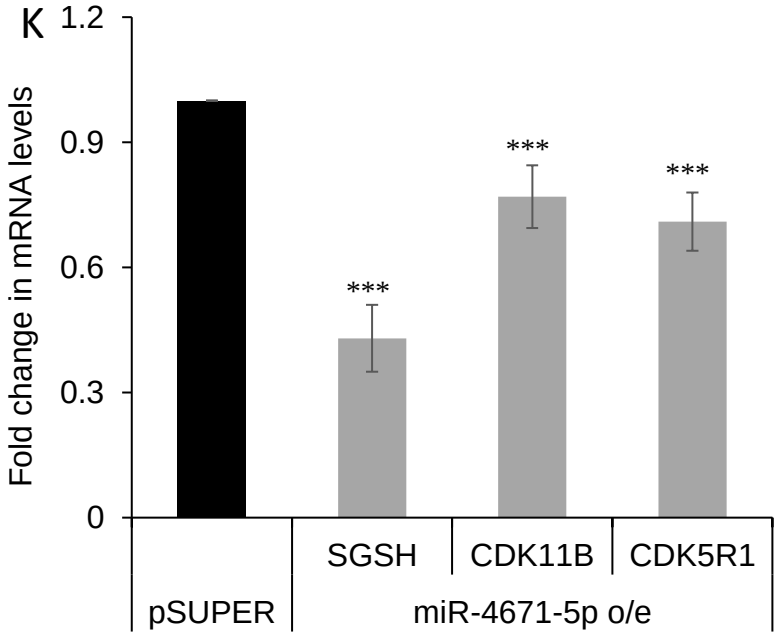
K
Fold change in mRNA levels
1.2
0.9
0.6
0.3
0
***
***
***
SGSH
CDK11B
CDK5R1
pSUPER
miR-4671-5p o/e

Figure 6

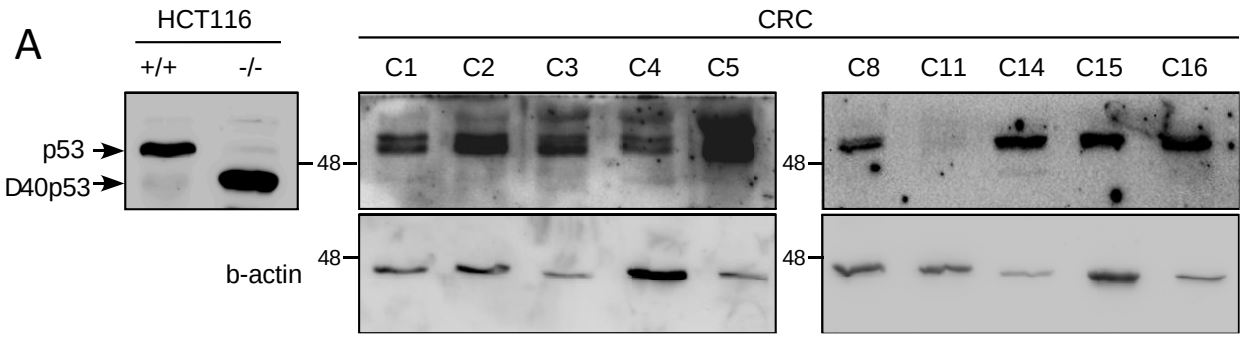
A
HCT116
+/+
-/-
CRC
C1
C2
C3
C4
C5
C8
C11
C14
C15
C16
p53
D40p53
48
b-actin

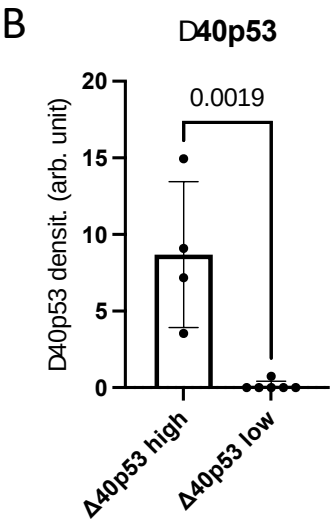
B
D40p53
D40p53 densit. (arb. unit)
0.0019
Δ40p53 high
Δ40p53 low

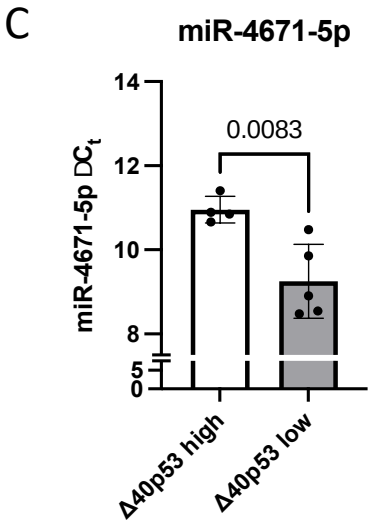
C
miR-4671-5p
miR-4671-5p DCt
0.0083
Δ40p53 high
Δ40p53 low

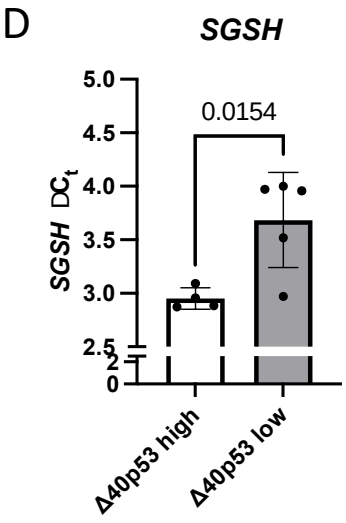
D
SGSH
SGSH DCt
0.0154
Δ40p53 high
Δ40p53 low

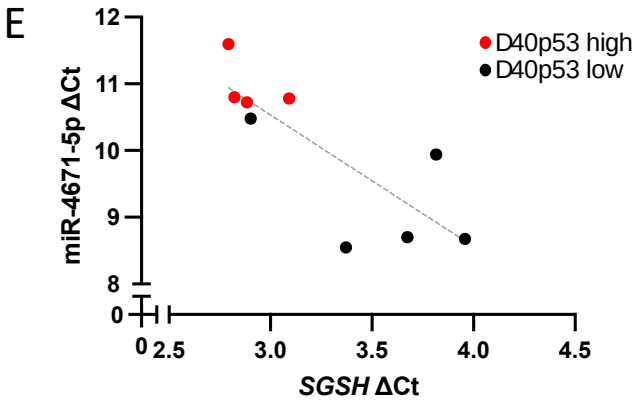
E
D40p53 high
D40p53 low
miR-4671-5p ΔCt
SGSH ΔCt

Figure 7

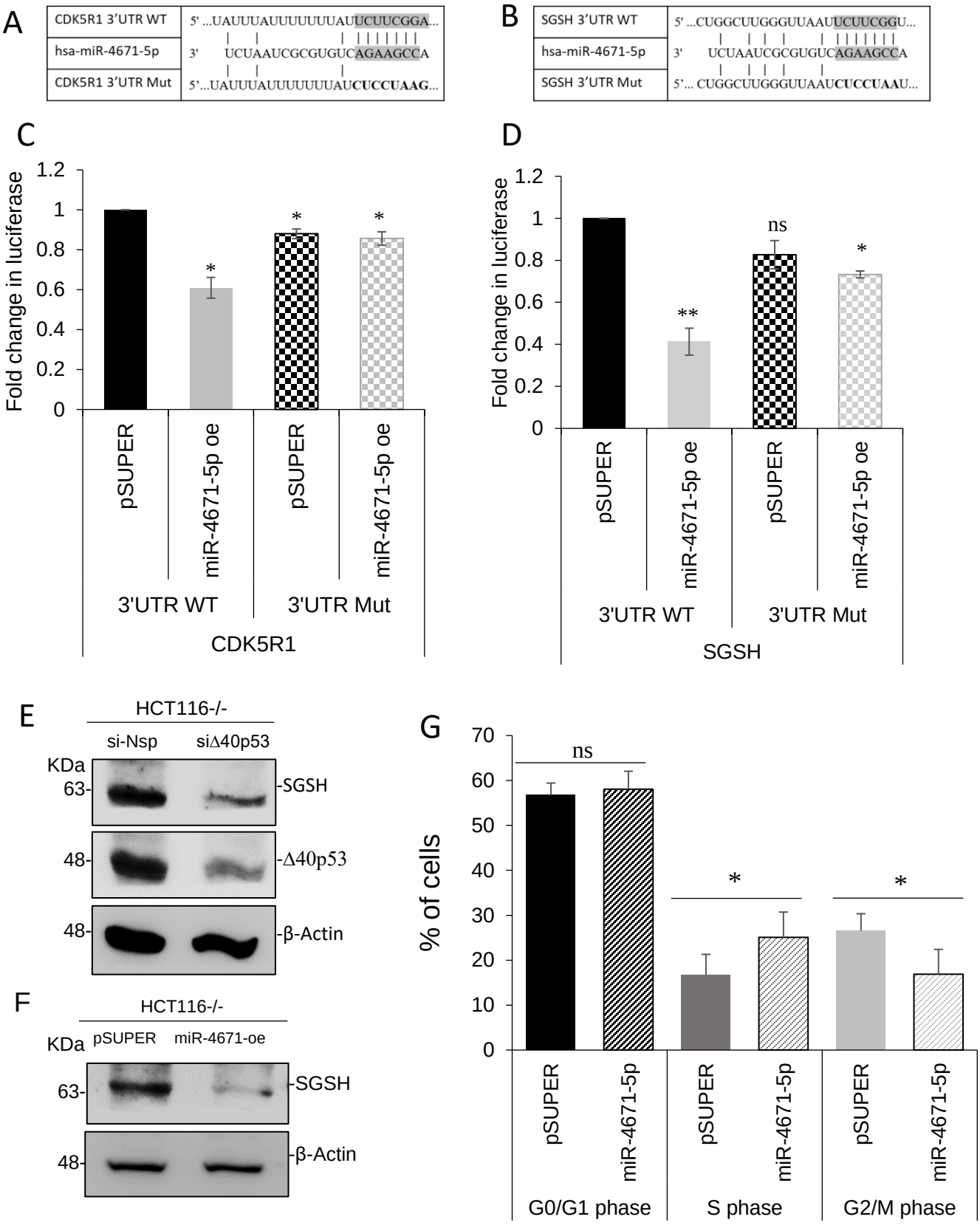
A
CDK5R1 3'UTR WT
5' ...UAUUUAUUUUUUUAUUCUUCGGA...
hsa-miR-4671-5p
3' UCUAAUCGCGUGUCAGAAGCCA
CDK5R1 3'UTR Mut
5'...UAUUUAUUUUUUUAUCUCCUAAG...
B
SGSH 3'UTR WT
5' ...CUGGCUUGGGUUAAUUCUUCGGU...
hsa-miR-4671-5p
3' UCUAAUCGCGUGUCAGAAGCCA
SGSH 3'UTR Mut
5'... CUGGCUUGGGUUAAUCUCCUAAU...
C
Fold change in luciferase
1.2
1
0.8
0.6
0.4
0.2
0
*
*
*
pSUPER
miR-4671-5p oe
pSUPER
miR-4671-5p oe
3'UTR WT
3'UTR Mut
CDK5R1
D
Fold change in luciferase
1.2
1
0.8
0.6
0.4
0.2
0
**
ns
*
pSUPER
miR-4671-5p oe
pSUPER
miR-4671-5p oe
3'UTR WT
3'UTR Mut
SGSH
E
HCT116-/-
si-Nsp
siΔ40p53
KDa
63-
-SGSH
48-
-Δ40p53
48-
-β-Actin
F
HCT116-/-
KDa
pSUPER
miR-4671-oe
63-
-SGSH
48-
-β-Actin
G
% of cells
70
60
50
40
30
20
10
0
ns
*
*
pSUPER
miR-4671-5p
pSUPER
miR-4671-5p
pSUPER
miR-4671-5p
G0/G1 phase
S phase
G2/M phase

Figure 8

A. Absence of Δ40p53

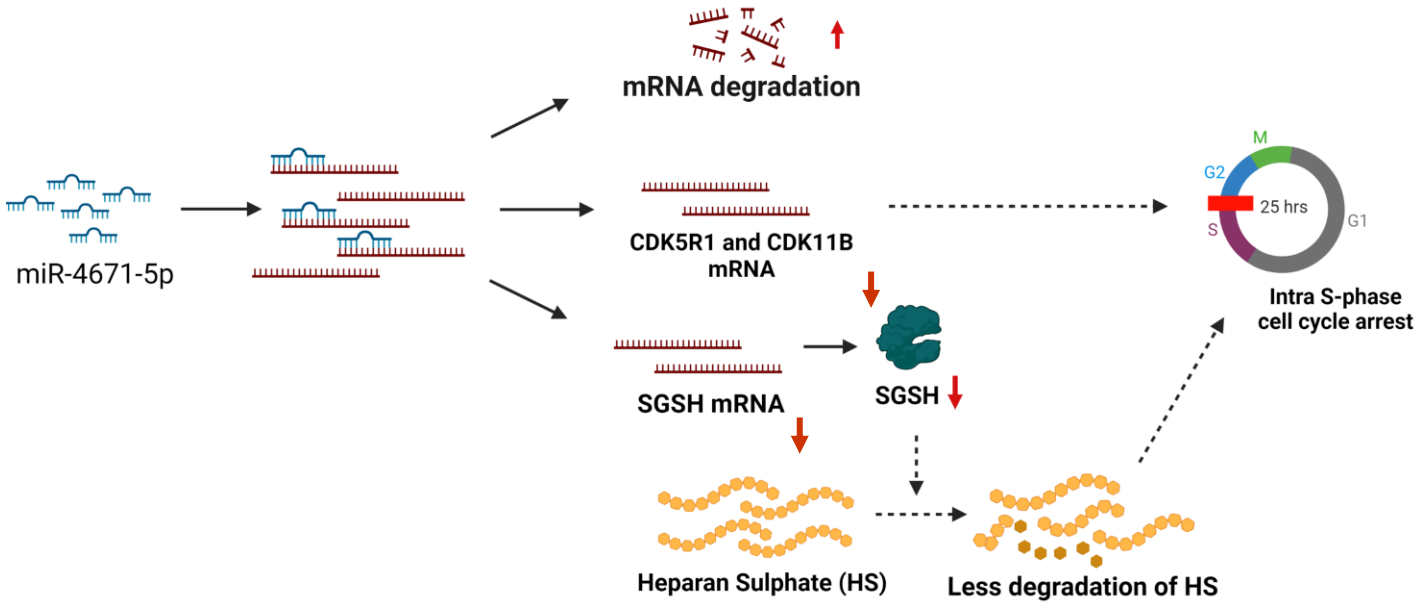
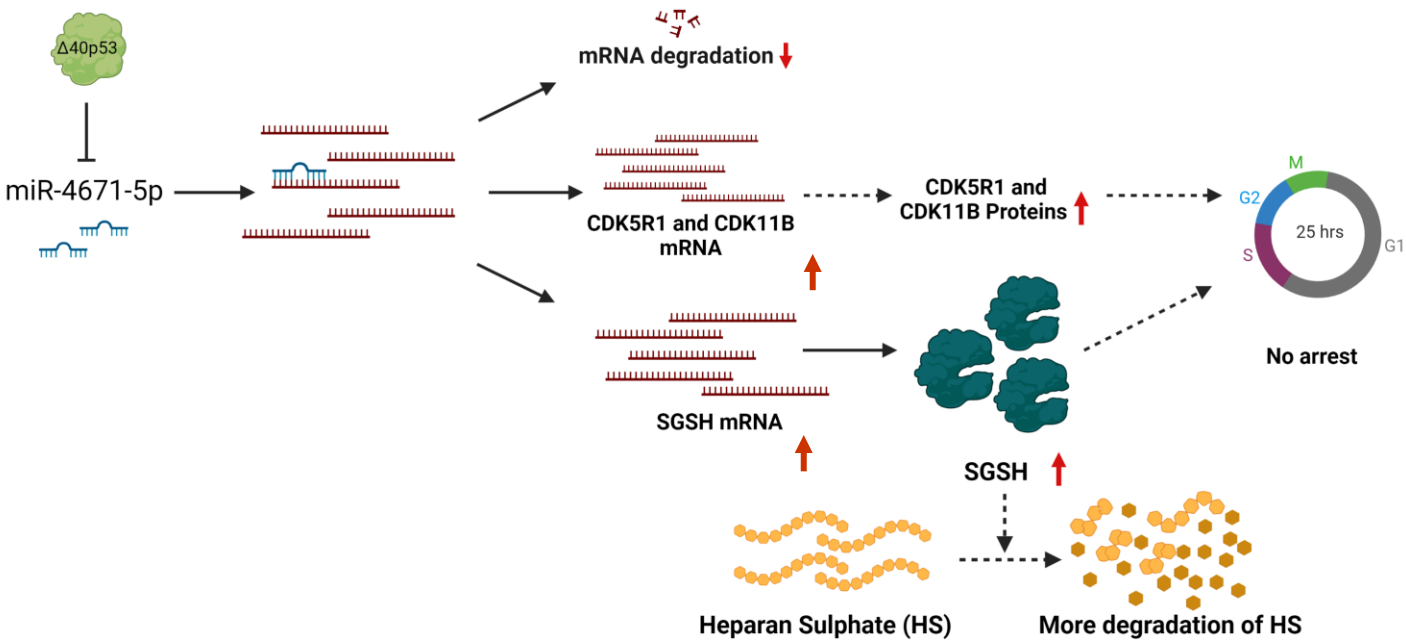
B. Presence of Δ40p53